AFWAL-TR-89-4004

LOW CYCLE FATIGUE OF SURFACE MOUNTED CHIP CARRIER/PRINTED WIRING BOARD JOINTS

H.D. Solomon

Materials Laboratory

Martin Marietta Corporatjon
Orlando, FLA 32855-6533

September 1987

Interim Report

Materials Laboratory
Air Force Wright Aeronautical Laboratories
Air Force Systems Command
Wright-Patterson Air Force Base, OH 45433-6553

Unclassified
SECURITY CLASSIFICATION OF THIS PAGE

ADA204191

REPORT DOCUMENTATION PAGE

Form Approved
OMB No. 0704-0188

1a. REPORT SECURITY CLASSIFICATION Unclassified	1b. RESTRICTIVE MARKINGS
2a. SECURITY CLASSIFICATION AUTHORITY None	3. DISTRIBUTION/AVAILABILITY OF REPORT Approved for Public Release; Distribution Unlimited
2b. DECLASSIFICATION/DOWNGRADING SCHEDULE None	
4. PERFORMING ORGANIZATION REPORT NUMBER(S) 87CRD185	5. MONITORING ORGANIZATION REPORT NUMBER(S) AFWAL-TR-89-4004
6a. NAME OF PERFORMING ORGANIZATION MARTIN Marietta Corp. 6b. OFFICE SYMBOL (If applicable)	7a. NAME OF MONITORING ORGANIZATION Materials Laboratory (AFWAL/MLTE) Air Force Wright Aeronautical Laboratories
6c. ADDRESS (City, State, and ZIP Code) P.O. Box 5837, Orlando, Florida 32855-5837	7b. ADDRESS (City, State, and ZIP Code) Wright-Patterson AFB, OH 45433-6533
8a. NAME OF FUNDING/SPONSORING ORGANIZATION Materials Laboratory 8b. OFFICE SYMBOL (If applicable) AFWAL/MLTE	9. PROCUREMENT INSTRUMENT IDENTIFICATION NUMBER F33615-85-C-5065
8c. ADDRESS (City, State, and ZIP Code) Air Force Wright Aeronautical Laboratories Wright-Patterson AFB, OH 45433-6533	10. SOURCE OF FUNDING NUMBERS PROGRAM ELEMENT NO. 78011F; PROJECT NO. 3095; TASK NO. 04; WORK UNIT ACCESSION NO. 02

11. TITLE (Include Security Classification)
Low Cycle Fatigue of Surface Mounted Chip Carrier/Printed Wiring Board Joints

12. PERSONAL AUTHOR(S)
Solomon, H.D.

13a. TYPE OF REPORT	13b. TIME COVERED	14. DATE OF REPORT (Year, Month, Day)	15. PAGE COUNT
Interim	FROM _____ TO _____	September 1987	53

16. SUPPLEMENTARY NOTATION

17. COSATI CODES			18. SUBJECT TERMS (Continue on reverse if necessary and identify by block number)
FIELD	GROUP	SUB-GROUP	
20	11		surface mount technology, chip carrier, PWB, low cycle fatigue joint cracking. (SDC)

19. ABSTRACT (Continue on reverse if necessary and identify by block number)

Chip carrier/printed wiring board joints have been tested isothermally, at 35°C, in shear. The joints were subjected to fully reversed cycling with fixed plastic displacement limits. The fatigue life was correlated to this displacement by a pseudo Coffin-Manson law. The fatigue life was defined in terms of a 25%,50%, 90%, and 100% drop in the load required to produce a given displacement. The resistance of each of 22 joints was also measured and N_f defined in terms of the first joint to increase by 0.02%,0.05%,0.1%,1%,10%,100%, and 10X.

The results were found to be in general agreement with those obtained previously on single, larger, solder joints. Some variations were noted in the Coffin-Manson exponent, depending on how the displacement and fatigue lives were defined. This was discussed along with a descriptive model describing the process of joint failure. A set of displacement vs. fatigue life curves is provided, which can be used to estimate the joint life based upon a variety of criteria. Keywords:

20. DISTRIBUTION/AVAILABILITY OF ABSTRACT	21. ABSTRACT SECURITY CLASSIFICATION
☒ UNCLASSIFIED/UNLIMITED ☐ SAME AS RPT. ☐ DTIC USERS	Unclasified

22a. NAME OF RESPONSIBLE INDIVIDUAL	22b. TELEPHONE (Include Area Code)	22c. OFFICE SYMBOL
Preston Opt	(513) 255-2461	AFWAL/MLTE

DD Form 1473, JUN 86 *Previous editions are obsolete.* SECURITY CLASSIFICATION OF THIS PAGE

LOW CYCLE FATIGUE OF SURFACE MOUNTED CHIP CARRIER/PRINTED WIRING BOARD JOINTS

H.D. Solomon

1. INTRODUCTION

The surface mounting of chip carriers (CCs), devices which hold the Si integrated circuit chips, has several advantages over the older process of soldering chip carrier leads into plated-through holes. Surface mounting entails soldering directly to lands on the printed wiring board (PWB). This reduces manufacturing costs, takes up less PWB space, and can be easily automated [1]. There is, however, an increased thermal fatigue problem with this type of attachment. This is especially true for leadless chip carriers where the chip carrier is soldered directly to the PWB. With no lead to take up the thermal strain developed by the difference in the coefficient of thermal expansion between the chip carrier and printed circuit board, surface mounted leadless chip carrier joints are particularly prone to thermal fatigue failure. This thermal fatigue results from the mismatch strain developed when the CC/PWB is thermally cycled. This problem has initiated a considerable amount of research into the fatigue of this type of joint [1-10]. One approach is to mechanically cycle these joints rather than producing the strains which cause failure by changing the temperature. This is the approach followed here – fatigue failures were produced in actual CC/PWB joints by mechanically cycling, at 35 °C, at different displacement levels.

2. EXPERIMENTAL PROCEDURE

2.1 Test Specimen Design and Production

Since a critical part of this program was to determine the behavior of CC/PWB joints, it was necessary to test actual joints made by typical processing techniques. The left hand side of Figure 1 shows the 44IO leadless chip carrier (Keocera #PB-81840) that was utilized. Typically, an Si device is soldered into the central well and attached to the inner pads by wire bonding; then a lid is soldered on the upper layer gold-plated square. In these experiments, however, no device was utilized in the chip carrier. Instead, a Cu return path plate was soldered to the inner pads, shorting them all together. A chip carrier with this Cu return path plate is also shown in Figure 1 (next to the as-received chip carrier). A hole was drilled into the Cu plate, and a Cu wire soldered to the plate and chip carrier. This soldering was done in conjunction with the soldering of the Cu plate to the inner chip carrier pads in a N_2 box on a hot plate. A 96.5 Sn/3.5 Ag eutectic solder was employed because it has a melting point of 221 °C, and thus it remains solid during the subsequent soldering of the chip carrier to the PWB, which was done at a lower temperature. A 1/8 in. (3.175 mm) thick glass polyimide PWB was utilized. Two ounce Cu was used to produce the circuitry shown in Figure

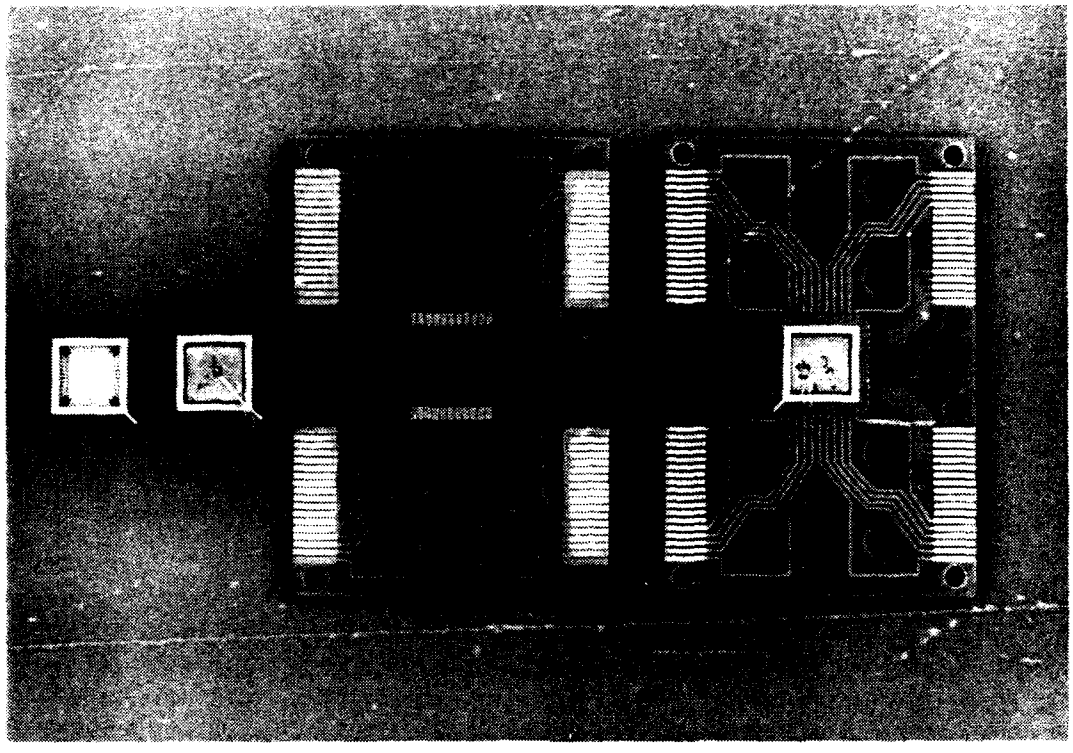

Figure 1. Chip Carrier, PWB and CC/PWB assembly.

1. A 0.002-0.003 in. (0.05-0.076 mm) solder mask (Dynachem DM) was put down over those areas that were not to be soldered.

Figure 1 (right-hand side) shows the chip carrier soldered to the printed circuit board. Only two opposite sides of the chip carrier have been soldered to the PWB (rather than using all 4 sides). Figure 2 shows a close-up of one of these two rows of joints. Each side of the CC contains 11 pads, so a total of 22 joints were made attaching the CC to the PWB. All of the joints discussed here were made by the vapor phase process in an HTC batch vapor phase unit operated at 423 °F (217 °C). The joints were made from Sn63 (63 wt% Sn/37 wt% Pb) solder paste (α metals lot #60523219), containing 90% solids and RMA384 flux. A 0.010 in. (0.025 mm) thick stencil was used when the paste was applied.

The paste was cured 1 hr. at 80 °C prior to the vapor phase soldering. A 30-second dwell in the primary temperature region (217 °C) was used to flow the solder, and a 3-minute dwell was used in the secondary region which was kept at 260-280 °F (127-138 °C) where the solidification took place. Final cleaning was done in Freon TMS. Prior to the soldering operation, both the chip carriers and printed wiring boards were pre-tinned by solder pot immersion with Sn63 solder.

2.2 Mechanical and Electrical Testing

The test board is inserted into slotted grips as shown in Figure 3. Spacer shims are used to position the solder joints so that they are at the center of the grip. This eliminates bending. It was not sufficient to just position the solder joint at the load line. A slotted grip is also necessary to symmetrically apply the load. In some preliminary tests, one or two specimens were bolted on the outside of a solid grip. In some tests, two specimens were used on the opposite faces of the grip, while on others, only a single specimen was used on one face. A few tests were also run with special asymmetric grips. Here the specimen was located at the load line, but the load was applied asymmetrically. These alternate gripping arrangements subjected the joints to varying degrees of bending; hence, they were replaced by the arrangement shown in Figure 3, which does not bend the joints to any significant degree. The results obtained with these alternate grips will be mentioned to show that, at least with the bending movements studied, bending does *not* appear to significantly influence the fatigue life.

The PWB has a slot under the chip carrier (see Figure 1). After the board is bolted into the grips, a carbide "Dremel" tool is used to enlarge the slot and separate the PCB into two sections. The cutting tool rotates at 30,000 rpm and the testing machine maintains a zero load throughout the cutting operation. To minimize any possible stresses being applied during the cutting operation, a steel backing plate is bolted to each grip half prior to cutting apart the PWB. The cut PWB is shown in Figure 4. Also shown in Figure 4 are the connectors that allow the resistance of each joint to be measured and the attachment to the Cu return path plate.

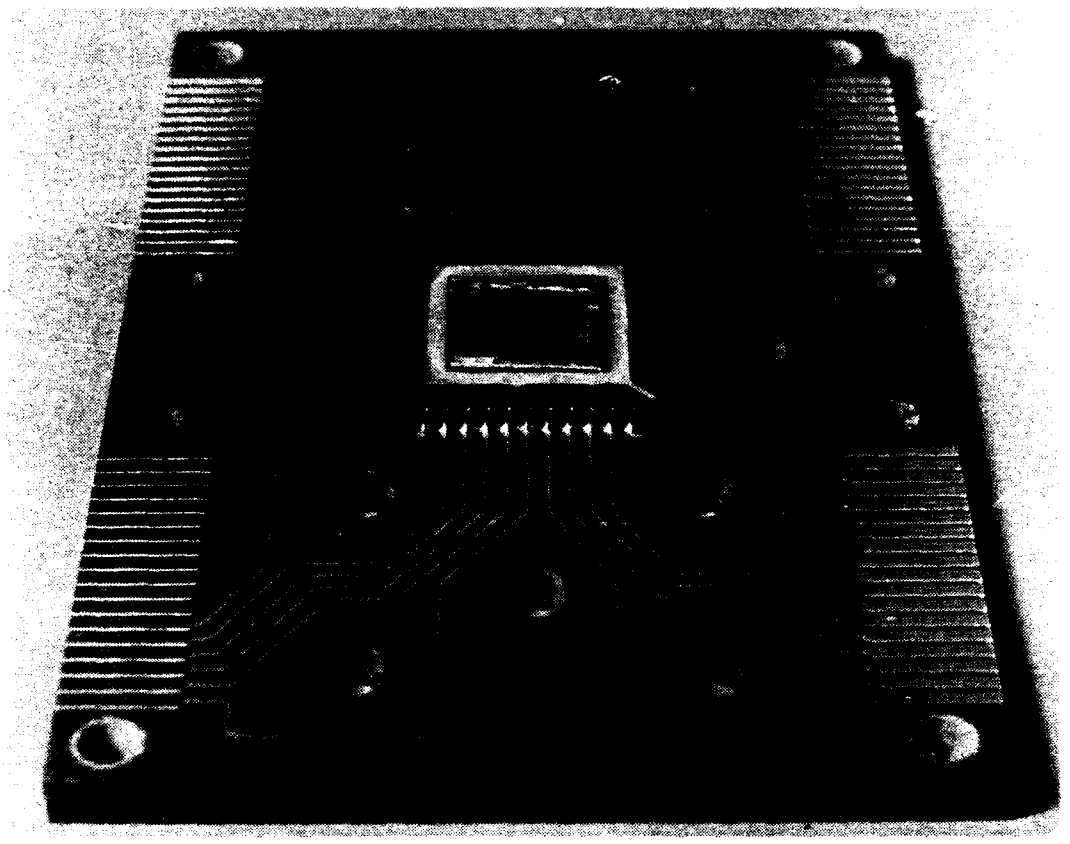

Figure 2. Close-up of one row of joints in the CC/PWB assembly.

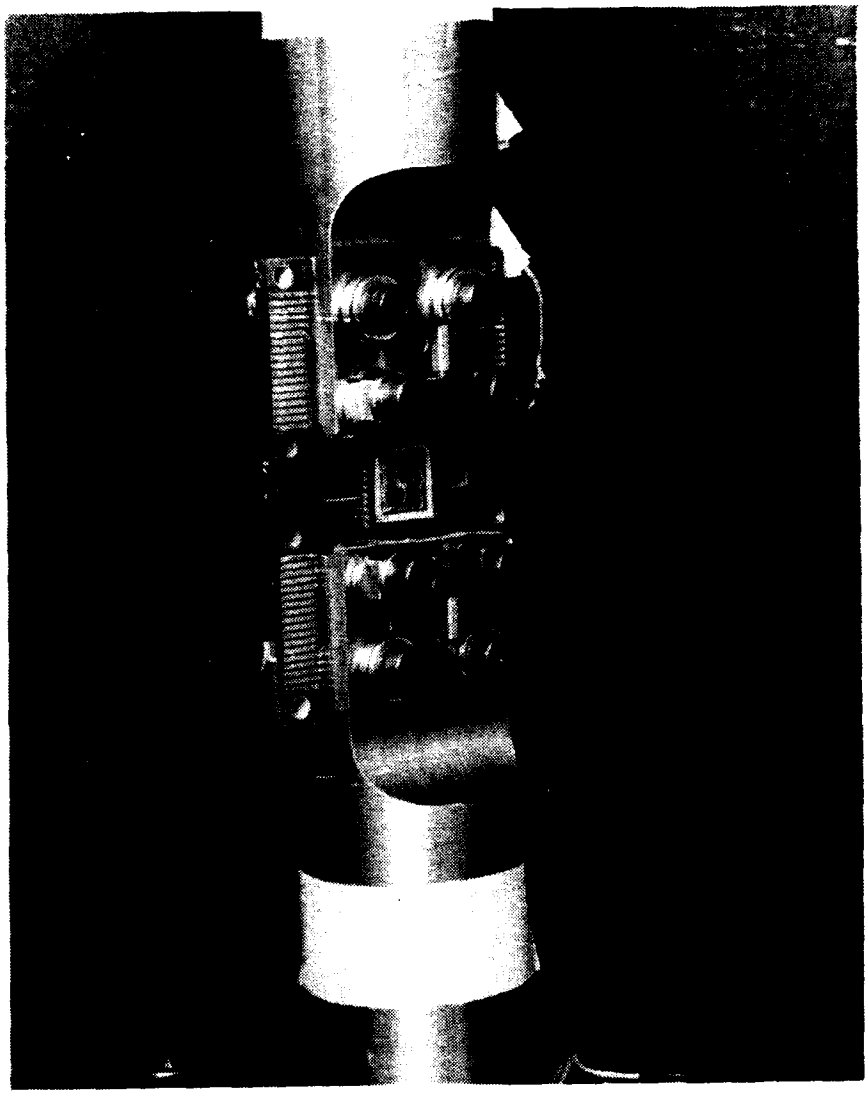

Figure 3. Test assembly in slotted grips.

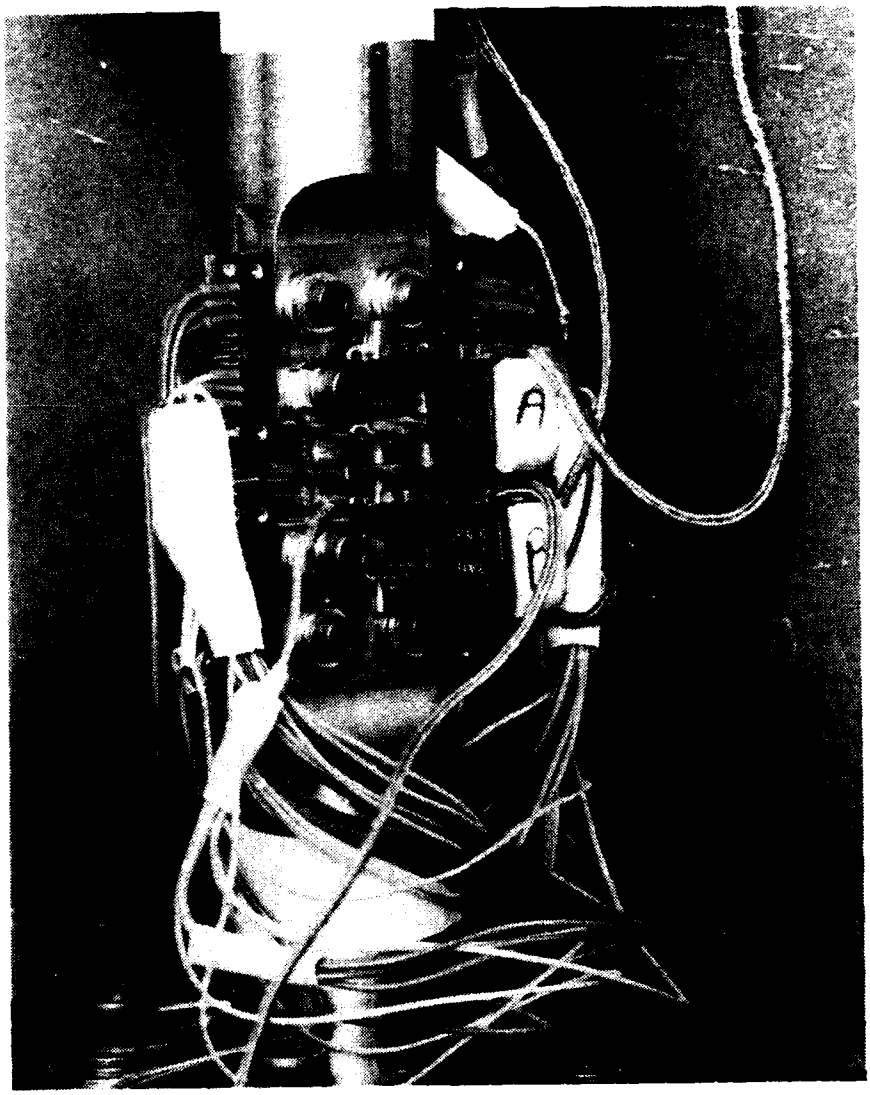

Figure 4. **Final assembly with two extensometers to measure the displacements across each row of joints.**

The displacement applied to the solder joints is measured by means of a clip-gage extensometer. Two methods were employed. In early tests, a single clip-gage was attached to the grips, across the chip carrier. The attachment posts are shown in Figure 3. In most tests, a more elaborate setup was employed. A yoke (held in place with set screws) was placed around the chip carrier. Two extensometers were employed with the yoke. One measured the displacement from the yoke across the top row of solder joints, and the other measured the displacement across the bottom row of joints. The yoke and extensometers are shown in Figure 4 and schematically in Figure 5b. Figure 5a shows the side view of the cut PWB prior to the yoke and extensometer attachment.

The load cell and extensometers provide the information about the load and displacement being applied to the specimen. An example of this load-displacement behavior is shown in Figure 6. Four types of hysteresis loops are shown in Figure 6. The applied load is shown vs. the $T+B$ displacement (i.e., the sum of the extensometer displacement across the top (T) and bottom (B) row of joints), vs. the T and B displacement separately and vs. the plastic component of the $T+B$ displacement. The plastic displacement is determined by subtracting out the linear load-displacement component from the $T+B$ displacement. This is done with an analog plastic strain computer. The plastic displacement signal Δ_p, is given by

$$\Delta_p = \Delta_{total}(T+B) - KP \qquad [1]$$

where $\Delta_{total}(T+B)$ is the sum of the output of the A and B extensometers, P is the applied load, and K is a constant which depends upon the elastic properties of the solder joint and the elastic properties of the PWB and CC. The plastic strain computer is adjusted for variations in K such that $\Delta_p = O$ for small, elastic, load excursions. The straight lines on the left-hand side of Figure 6 show load-Δ_T and load-Δ_p lines for such a load excursion.

The possibility that the observed non-linear load displacement behavior could be due to non-solder behavior was checked by straining an unseparated PWB which did not contain a chip carrier or slit. This board was loaded at room temperature to ± 100 lb with no non-linear strains being produced. The elastic modulus measured from the observed load displacement slope was 1.7×10^6 psi which, while lower than the expected value of about 3×10^6 psi, is not unreasonable. The handbook elastic modulus values range from about 2.5×10^6 psi to 3.5×10^6 psi, but variations in the fiber content and strain rate may increase or decrease measured modulus outside this range. The higher the glass content and the greater the strain-rate, the greater will be the modulus. Modulus measurements made by measuring the velocity of sound or mechanically cycling at high frequencies should be expected to be higher than those measured here, where a relatively low cycling frequency of 0.3 Hz was employed. A small amount of bending may also contribute to this lower measured modulus.

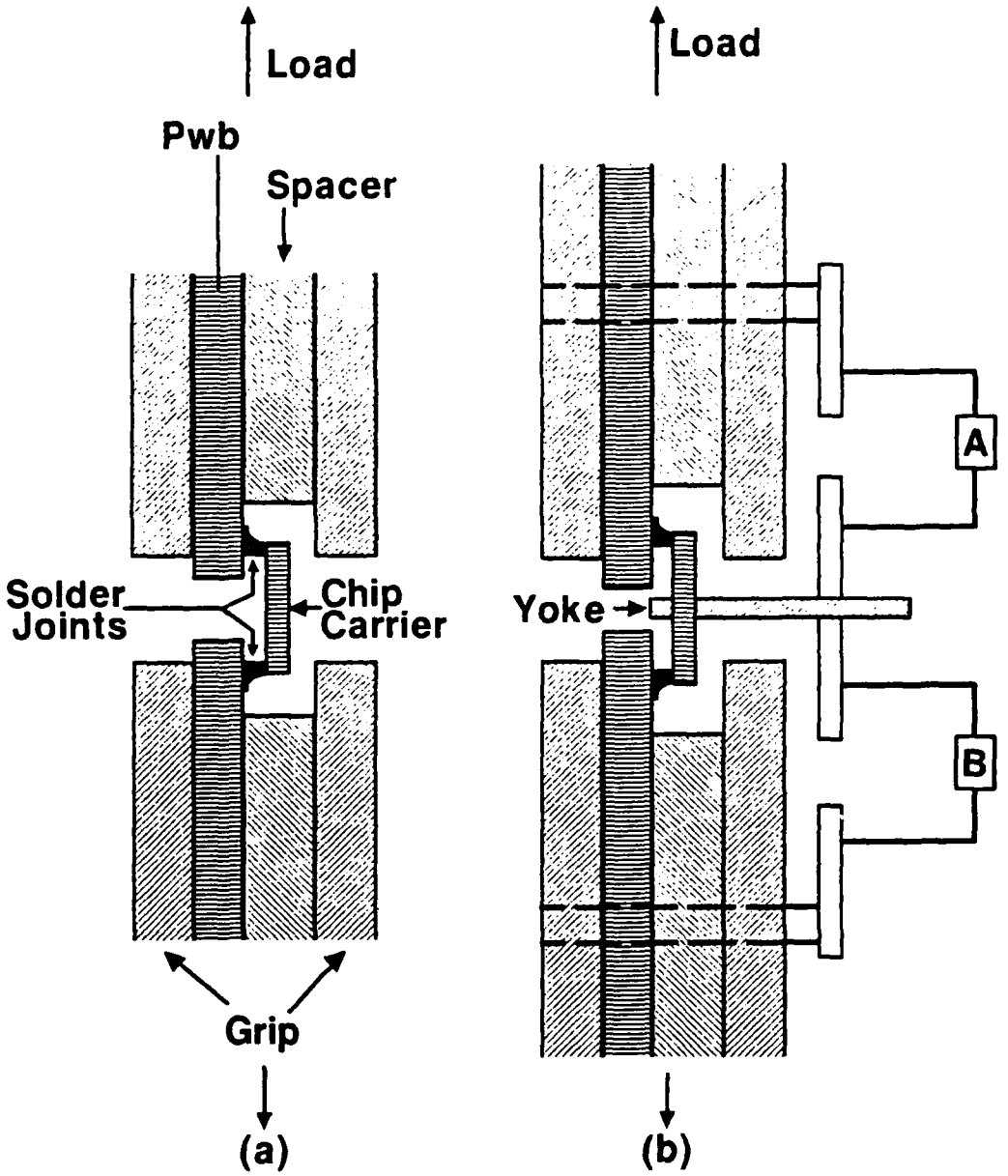

Figure 5. **Schematic showing the test assembly. (a) Without the yoke and extensometer, and (b) with yoke and extensometers.**

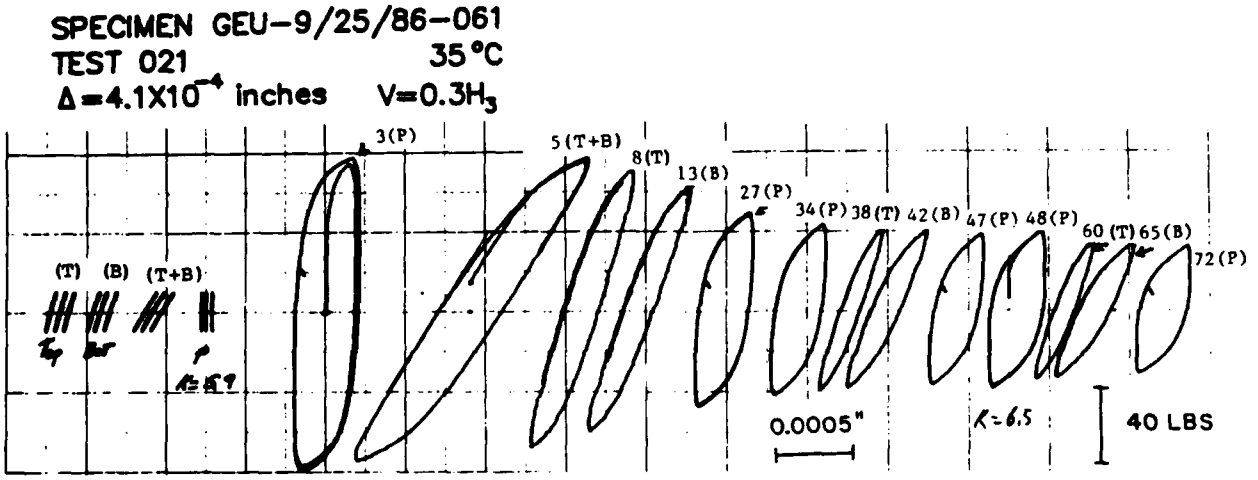

Figure 6. Hysteresis loops.

The experiments described here were run with fully reversed plastic displacement limits, under total displacement feedback control. The crosshead motion was controlled by the $\Delta_T(T+B)$ signal and was reversed when a predetermined level of plastic displacement $(+p)$ was reached (i.e., at a plastic displacement limit). The crosshead motion continued in this reversed direction until the other plastic displacement limit $(-p)$ was reached, whereupon the crosshead was reversed again. The absolute values of the plastic strain limits were equal, i.e., $+p = |-p|$ so that the cycling was fully reversed about a mean of zero plastic displacement. Figure 6 shows experiments where the plastic displacement range Δ_p (i.e., the hysteresis loop width) was,

$$\Delta_p = p + |-p| = 4.1 \times 10^{-4} \text{in.} (1.04 \times 10^{-2} \text{mm}) \quad [2]$$

The cycling frequency was kept at about 0.3 Hz.

Figure 6 shows that the load range required to produce the plastic strain range Δ_p decreased with cycling. This load drop is indicative of fatigue cracking [2]. The load drop illustrates the average cracking, averaged over all 22 joints being tested.

The test was stopped periodically and the resistance on each joint was measured individually, thus revealing the cracking behavior of each joint. The resistance was measured by passing a 0.100 A current individually through each joint and individually measuring the voltage drop. The voltage drop was measured by an HP Model 3456A DVM operated by an HP 3497A Data Acquisition and Control system under the overall control of an HP 9000/300 computer. The system feeds current through one joint for one second, then reverses the current flow for another second before switching current to the next joint. The reversing of the current is done to average out thermal EMF's. The current is fed through the thick leads (see Figure 1) to the PWB pad, through the solder joint, through the conductive metallization in the chip carrier, to the Cu return path plate, through the wire soldered to the plate, to a connection with the power supply. The voltage drop was measured through the thinner leads to the same PWB pad, as the current is flowing through the solder joint, chip carrier, Cu return path plate, lead wire, and then to the DVM. The DVM averages the voltage of the last 0.8 second of each one-second scan. The first 0.2 second is disregarded to allow for transients to settle out. The current was determined by measuring the voltage drop through a calibrated precision resistor. The current was measured before and after measurements were made on each row of joints, and the average current was used in calculating the resistance from the individual voltage drop measurements. The voltage drop through a dummy specimen, placed within the test chamber, was also made so that the resistance change due to temperature changes could be corrected for. Table 1 shows the results of a typical resistance scan. In this case the test was stopped after 207 cycles. By this time the load had dropped by 80.9%. This was the seventh time the test was stopped for a resistance measurement. Table 1a lists the printout displayed at the time the measurements were taken. Table 1b lists

the printout summary after the test has been completed. The left-hand column lists the joint number from the top 1-11 to the bottom 1-11 (the prefix R is a hold-over from an early set of experiments where two PWB's were tested and the set of connectors being employed was used on the right-hand specimen).

Table 1a lists the voltage drop for each joint and the ratio with the first measurement (from Scan #1). Also shown are the measured current and the ratio with the value obtained on the first run (Scan #1). The voltage for the dummy and the ratio with the first measurement are also shown. After each scan, the voltages are converted into calculated resistances (by dividing by the average of the current measured before and after each group of voltage measurements). These resistance measurements are printed out after the test is completed, as shown in Table 1b. The resistance, resistance ratio with that measured in Scan #1 for that joint, and the ratio of the ratios of the joint resistance and dummy are listed in the printout for each scan.

Table 2 is a summary of the data for each joint and each scan. Here, the scan number (Sc), cycle number, load drop, and the ratio of resistance ratio and dummy ratio minus 1 are shown. To accommodate all the data, the resistance ratio data is shown rounded to only four significant figures. When actually working with the data, the more accurate data for each individual scan is used (see 1b). A change in resistance of 1×10^{-4} can be resolved. With a resistance of approximately 0.1 ohm this means that approximately 10×10^{-6} ohms can be resolved.

The load drop and resistance increase for the hysteresis loops of Figure 6 and resistance measurements of Tables 1 and 2 are shown in Figure 7. Here, $1-(\Delta P/\Delta P_{max})$ and $(R/R_o/R_D/R_{Do})-1$ are shown vs. the cycle number, where ΔP is the hysteresis load range at cycle N, ΔP_{max} is the maximum hysteresis load range, R/R_o the ratio of the resistance at cycle N to the initial resistance, and R_D/R_{Do} is the ratio of the resistance of a dummy joint at cycle N to the initial dummy resistance (this term corrects for temperature change variations in R). The load drop term varies from zero at $\Delta P = \Delta P_{max}$ to 1 when $\Delta P = O$. This resistance parameter varies from zero at $R = R_o$ and $R_D = R_{Do}$ to a maximum value of about 25, reached when an open circuit is produced (at an open circuit, a 25 volt system compliance voltage is read rather than an infinite voltage because of the infinite resistance).

The resistance change for the three joints showing the largest change, the joint showing the median change, and the joint showing the least change are all plotted. This sort of plot was made for each experiment, and from it the fatigue life, as determined by several criteria, was determined. The criteria of 25%, 50%, 90% and 100% drop in load were utilized, as were resistance increases (for the joint showing the greatest increase) of 0.02%, 0.05%, 0.1%, 1%, 10.0%, 100%, and 10×. In most experiments (but not the one illustrated in Figure 6), the test was continued until the load dropped by at least 90%, and one joint exhibited at least a 100% increase in resis-

Table 1

Results For A Typical Resistance Scan

(a) Printout Display Given During the Test

```
SCAN#= 7  14 Oct 1986          15:02:02
CYCLE NUMBER = 207      LOAD DROP = .809
     CURRENT =   .10035  AMPS---- I/I0 CURRENT= 1.00003
RT1        .01379240  VOLT      (V/V0) =     1.00054518
RT2        .01187200  VOLT      (V/V0) =     1.00050921
RT3        .01115415  VOLT      (V/V0) =     1.00049636
RT4        .01016165  VOLT      (V/V0) =     1.00052399
RT5        .01001595  VOLT      (V/V0) =     1.00053144
RT6        .00994960  VOLT      (V/V0) =     1.00043430
RT7        .01015160  VOLT      (V/V0) =     1.00042096
RT8        .01002790  VOLT      (V/V0) =     1.00036114
RT9        .01081390  VOLT      (V/V0) =     1.00037277
RT10       .01181320  VOLT      (V/V0) =     1.00039731
RT11       .01314565  VOLT      (V/V0) =     1.00042295
     CURRENT =   .10035  AMPS---- I/I0 CURRENT= 1.00003
RB1        .01429705  VOLT      (V/V0) =     1.00164789
RB2        .01265505  VOLT      (V/V0) =     1.00120663
RB3        .01167725  VOLT      (V/V0) =     1.00122094
RB4        .01094580  VOLT      (V/V0) =     1.00155837
RB5        .01055290  VOLT      (V/V0) =     1.00138793
RB6        .01059410  VOLT      (V/V0) =     1.00195080
RB7        .01063310  VOLT      (V/V0) =     1.00293124
RB8        .01094180  VOLT      (V/V0) =     1.00246276
RB9        .01221160  VOLT      (V/V0) =     1.01242732
RB10       .01553635  VOLT      (V/V0) =     1.04898277
RB11       .06207955  VOLT      (V/V0) =     3.81706075
     CURRENT =   .10035  AMPS---- I/I0 CURRENT= 1.00003
DUMMY         .01615  VOLT      (V/V0) =      .99994
```

(b) Final Printout Given at the End of the Tests

```
SCAN#= 7    CYCLE #=  207       LOAD DROP=  .809     TEMP.= 34.8 DEG. C
                R                  R/Ro              R/Ro/RD/RDo
 RT1            .1374             1.0005              1.0006
 RT2            .1183             1.0004              1.0005
 RT3            .1112             1.0004              1.0005
 RT4            .1013             1.0005              1.0006
 RT5            .0998             1.0005              1.0006
 RT6            .0991             1.0004              1.0005
 RT7            .1012             1.0004              1.0005
 RT8            .0999             1.0003              1.0004
 RT9            .1078             1.0003              1.0004
 RT10           .1177             1.0003              1.0004
 RT11           .1310             1.0004              1.0005
 RB1            .1425             1.0016              1.0017
 RB2            .1261             1.0012              1.0013
 RB3            .1164             1.0012              1.0013
 RB4            .1091             1.0015              1.0016
 RB5            .1052             1.0013              1.0014
 RB6            .1056             1.0019              1.0020
 RB7            .1060             1.0029              1.0030
 RB8            .1090             1.0024              1.0025
 RB9            .1217             1.0124              1.0125
 RB10           .1548             1.0489              1.0490
 RB11           .6186             3.8169              3.8172
DUMMY 1      .160962189782       RD/RDo= .999906228886
```

Table 2

Summary For All Scans

SUMMARY OF SPECIMEN # GEU-9/25/86-061R 14 Oct 1986-15:06:25
DATA STORED AS FILE NAME 021 ON DISK

SC	CYCLE	LOAD	RT1	RT2	RT3	RT4	RT5	RT6	RT7	RT8	RT9	RT10	RT11
1	3	0.000	0.000	0.000	0.000	0.000	0.000	0.000	0.000	0.000	0.000	0.000	0.000
2	27	.388	0.000	0.000	0.000	0.000	0.000	0.000	0.000	0.000	0.000	0.000	0.000
3	47	.528	0.000	0.000	0.000	0.000	0.000	0.000	0.000	0.000	0.000	0.000	0.000
4	72	.596	0.000	0.000	0.000	0.000	0.000	0.000	0.000	0.000	0.000	0.000	0.000
5	103	.681	0.000	0.000	0.000	0.000	0.000	0.000	0.000	0.000	0.000	0.000	0.000
6	151	.750	0.000	0.000	0.000	0.000	0.000	0.000	0.000	0.000	0.000	0.000	0.000
7	207	.809	0.000	0.000	0.000	0.000	0.000	0.000	0.000	0.000	0.000	0.000	0.000
SC	CYCLE	LOAD	RB1	RB2	RB3	RB4	RB5	RB6	RB7	RB8	RB9	RB10	RB11
1	3	0.000	0.000	0.000	0.000	0.000	0.000	0.000	0.000	0.000	0.000	0.000	0.000
2	27	.388	0.000	0.000	0.000	0.000	0.000	0.000	0.000	0.000	0.000	0.000	0.000
3	47	.528	.001	.001	.001	.001	0.000	0.000	0.000	0.000	0.000	.001	.001
4	72	.596	.001	.001	.001	.001	.001	.001	.001	.001	.001	.001	.001
5	103	.681	.001	.001	.001	.001	.001	.001	.001	.001	.002	.002	.002
6	151	.750	.001	.001	.001	.001	.001	.001	.002	.002	.005	.005	.012
7	207	.809	.002	.001	.001	.002	.001	.002	.003	.002	.012	.049	2.817

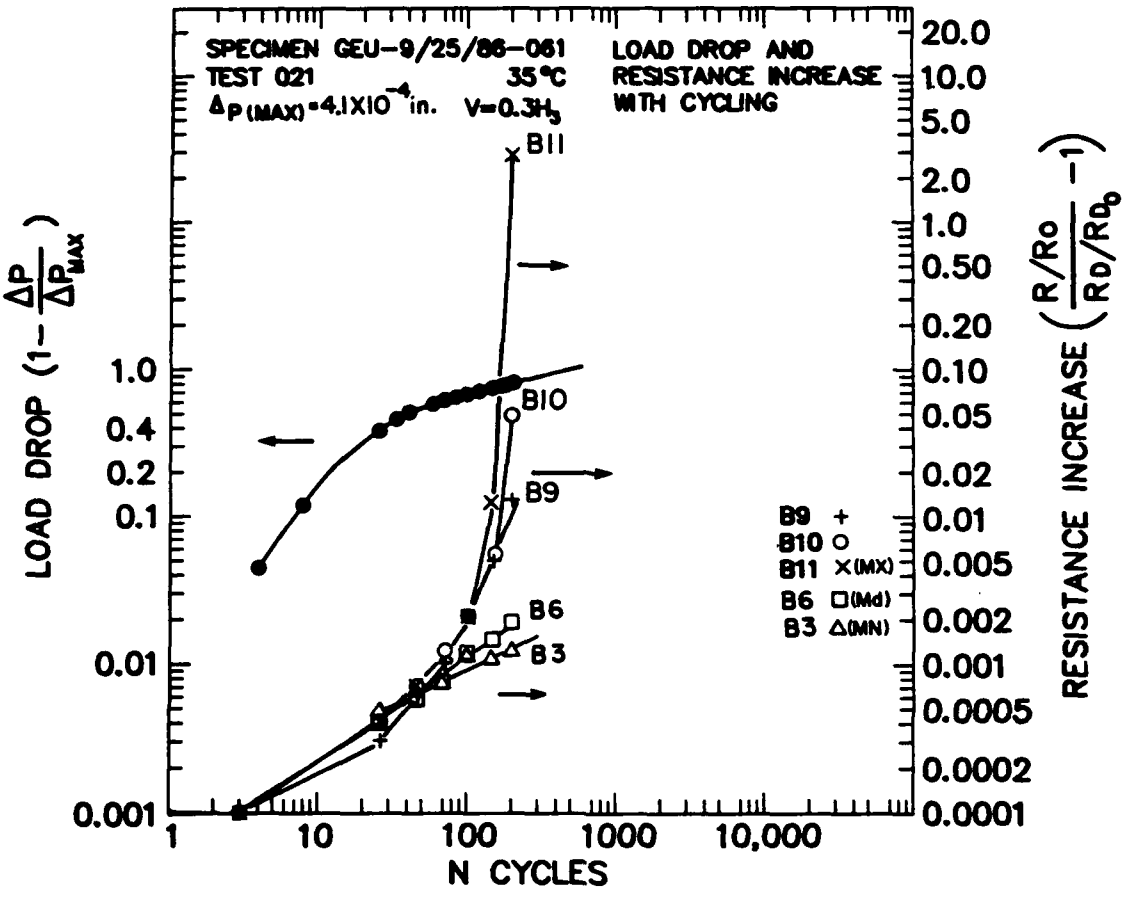

Figure 7. Load drop and resistance increase with cycling.

tance. Where the test was stopped short of this level, the data was extrapolated to the closest failure criteria. For instance, if the maximum resistance increase was greater than 5% but less than 10%, the data would be extrapolated to enable the determination of the number of cycles for a 10% resistance increase but not further. If the maximum resistance increase was less than 5%, then an extrapolation to 10% would not be made.

2.3 Choice of Control Limit Variable

Several choices could have been made to establish the variable to use to limit the fatigue cycling. The tests could have been run with load limits, i.e., cycled to a particular load, then reversed to reach another load limit. The tests could have been run with total displacement limits. Instead, plastic displacements were employed. This choice was dictated by the nature of the actual sort of fatigue cycle a solder joint experiences and by features of the experimental setup. Load limits are easy to apply and are justified in many applications but *not* in situations where thermal fatigue is important. Thermal fatigue results from the thermal mismatch between the chip carrier and PWB. This mismatch applies a displacement to the solder joint so a displacement limit is most appropriate to develop data to describe this sort of fatigue.

Since the solder experiences the application of a displacement, it might be expected that a total (elastic plus plastic) displacement would be the most appropriate type of limit to use. It is *not* for two reasons. The magnitude of the elastic strain that the solder experiences is dependent upon the rate of straining. Solder is a viscous material and the strain rate dependence of the flow stress is large [3,4]. At the high strain rates employed in these tests, the elastic strain is larger than that applied at the slower strain rates generally experienced during a thermal fatigue cycle. If a total displacement limit were used, then the amount of plastic displacement, which produces the fatigue damage, would vary with the applied strain rate. To overcome this, the plastic displacement was chosen as the control limit.

The choice of plastic displacement as the control limit was also necessitated by changes in compliance that occur throughout the test. If the total displacement is used as the control variable, then as the load drops throughout the test the amount of plastic displacement increases to compensate for decreases in the elastic displacement. The degree to which this happens depends upon the amount of machine elastic strain being measured. If no machine elastic displacement is measured, then the compliance change self-corrects and the plastic displacement remains constant even if the total displacement is used as the control limit [2]. If, however, the machine elastic displacement dominates, then all of the elastic displacement will be converted into plastic displacement when a total displacement limit is employed [2]. An intermediate situation exists in these solder joint experiments. The average compliance (displacement/load measured in the elastic range) is $7.20 \pm .21 \times 10^{-6}$ in/lb. This compliance is made up of

four contributions: elastic solder displacements of both rows of joints, PWB displacements, CC displacements and testing machine contributions (i.e., measured bending). The elastic measurements, discussed previously, on PWB's which have not been split apart yield a PWB and machine contribution to the total compliance of about 1.5×10^{-7} in/lb. The calculated compliance contribution of the CC is about 8.3×10^{-7} in/lb. Thus, 2.33×10^{-6} in/lb of the measured compliance is not due to solder deflections. This means that 4.87×10^{-6} in/lb is due to the solder or that the measured compliance of 7.205×10^{-6} in/lb is about 68% due to the solder. This is a higher contribution than was found in previous tests [2].

The high solder contribution to the measured compliance presents some problems because as cracking continues, the compliance increases (because the solder load bearing area decreases) but the control compliance is not increased. This, as illustrated in Figure 6, causes the control plastic strain to *decrease*. (As the compliance increases, the plastic strain computer is not subtracting out all of the elastic displacements. As this elastic contribution increases, the plastic contribution decreases because the control variable is being kept constant). This effect is mitigated by the fact that only about 68% of the compliance is due to the solder and the non-solder contributions do not change. Additionally, in a typical experiment, the fatigue cracking is confined to only one row of joints, so the compliance change will be only one-half that if both rows cracked. The net effect of these factors is that only about 34% of the load drop should contribute to this decrease in plastic displacement. The higher the plastic displacement limit, the less important is any contribution of changes in this limit due to the compliance change caused by the load drop. The decrease in plastic displacement only becomes significant when small plastic displacement limits (less than about 5×10^{-4} in. (1.27×10^{-2} mm)) are employed and the load decreases by more than one-half. The data has been corrected for this effect, as will be discussed later. If total displacement limits were used, then 66% of the load drop would have contributed to a plastic displacement increase and the influence of the compliance change would have been twice as great as was encountered here, where the plastic displacement limit was employed.

3. RESULTS AND DISCUSSION

3.1 Joint Cracking Behavior

Figure 7 shows that as the fatigue cycling continues, the hysteresis load decreases (Figure 7 uses a dimensionless function which increases from 0 to 1 as the load decreases) and the joint resistance increases. These changes are due to the development of fatigue cracks in the solder joints. Before we consider the correlations of the load drop and resistance increase with the applied displacement range, it is necessary to consider the metallographic and optical record of the joint cracking behavior.

While most of the fatigue tests were run until the load dropped by about 90% or the resistance increased appreciably, some tests were stopped before either of these occurrences. Figure 8 shows the cross-section of a joint which was cycled until the load decreased by 31%. As can be seen, a fatigue crack has developed under the chip carrier but has not yet grown through the fillet. The maximum joint resistance increase was 0.02% with most joints showing a resistance increase of 0.01% or less. In no case was a crack observed on the surface of the fillet.

Figure 8 illustrates that in the early stages of fatigue, the cracking is confined to the area under the chip carrier, where, in the case of the joint that was examined, a void was present. Voids under the chip carrier are the rule in these joints, which were made with solder paste. Gases evolved from the paste cannot escape, and they create the voids. These voids need not be detrimental; in fact they served a beneficial purpose in the joint illustrated in Figure 8. The initial cracking is believed to have started at the back end of the joint as a crack in the metallization of the chip carrier. When this crack hit the void, it was stopped, and then it restarted as a crack in the solder itself. The void acts as a crack stopper; it moves the crack away from the metallization on the region directly adjacent to the chip carrier. Metallization cracking and crack stoppage by a void are also illustrated in Figure 9. Here two solder pads are shown at low magnification. The transition from the grey to light region in the right-hand pad is shown at a high magnification in Figure 9b. The grey region is composed of W and Al_2O_3 crystals, which mark it as the chip carrier metallization. The failure in the solder looks ductile with no presence of fatigue striations. No striations could be expected in high strain cycling of such a ductile material. The transition from the metallization crack to the solder occurs at a void, which is typical. Figure 9 also illustrates another typical feature. While metallization cracks were observed at some joints, this phenomenon was by no means dominant. Figure 9 shows an adjacent joint where no metallization cracks were present. In fact, out of 12 specimens broken apart to reveal their fracture surfaces, metallization cracks were noted in only five specimens, and in these the cracks were located at the edges of only some of the joints tested. Other conditions, not discussed here, for instance testing at -55 °C, can make metallization cracking a predominant feature of the tests.

Figure 9 also shows that while voids predominate under the chip carrier, they can be present at the edge of the chip carrier, near the fillet (see the right-hand joint in Figure 8a). Voids were not, however, noted in the fillet itself, where they would have played a greater role in influencing the fatigue life.

The joints shown in Figure 10 were cycled until the load dropped by 60%. The joint of Figure 10a showed a resistance increase of 0.3%, and a crack is clearly visible. The joint of Figure 10b experienced a resistance increase of 0.15%, and a fine crack is visible. The joints of Figures 10c and 10d show the evidence of surface damage and

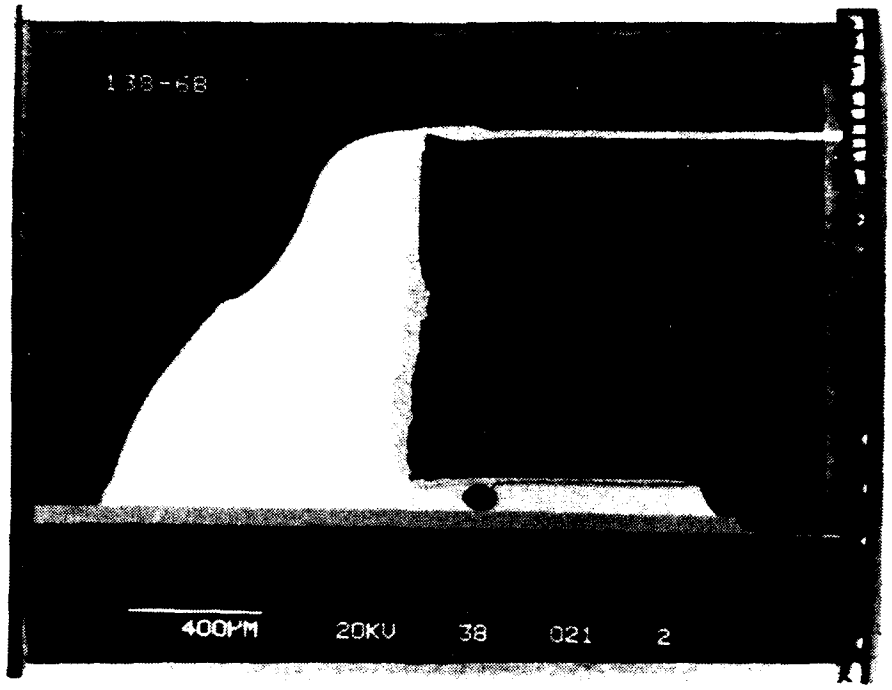

(a)

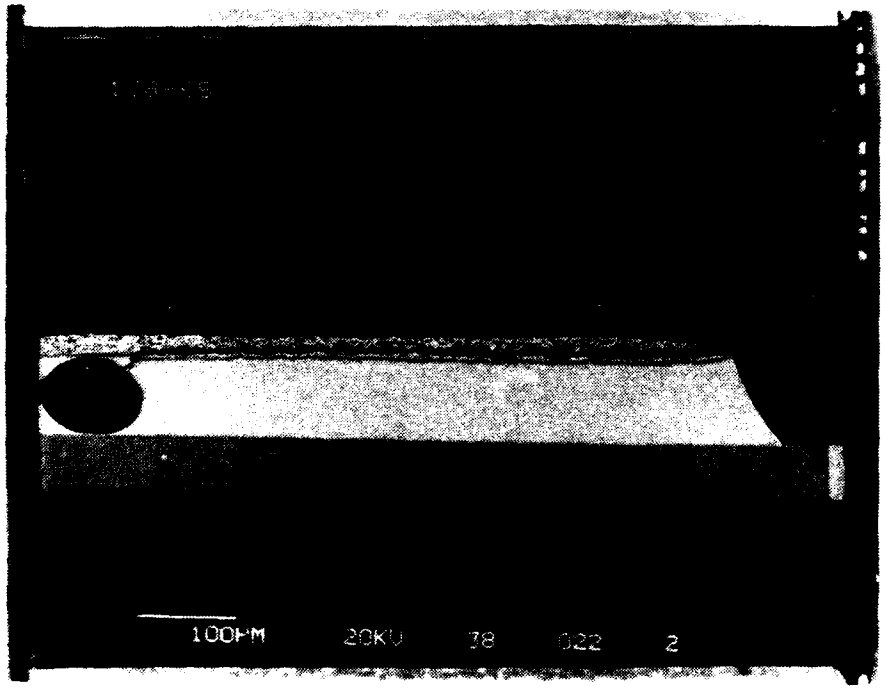

(b)

Figure 8. Cross-section of a joint cycled to a 31% drop in load. (a) Low magnification showing the entire joint, (b) higher magnification.

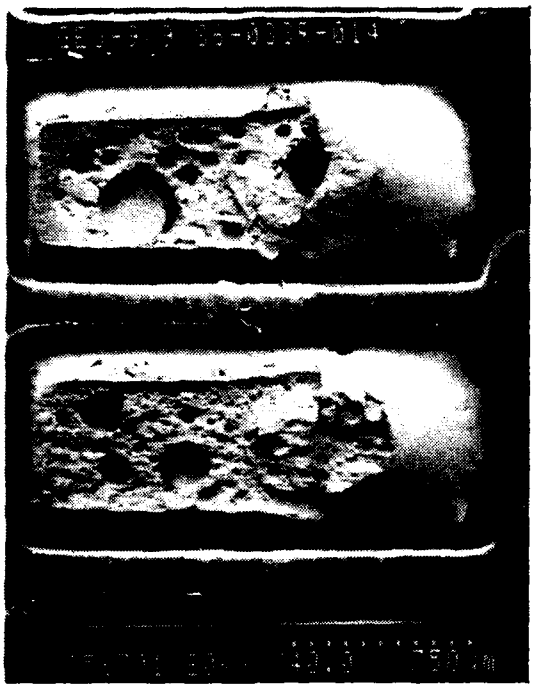

(a)

(b)

Figure 9. Fracture surfaces. (a) Two adjacent joints, one of which exhibited a metallization failure, (b) close-up of the metallization failure.

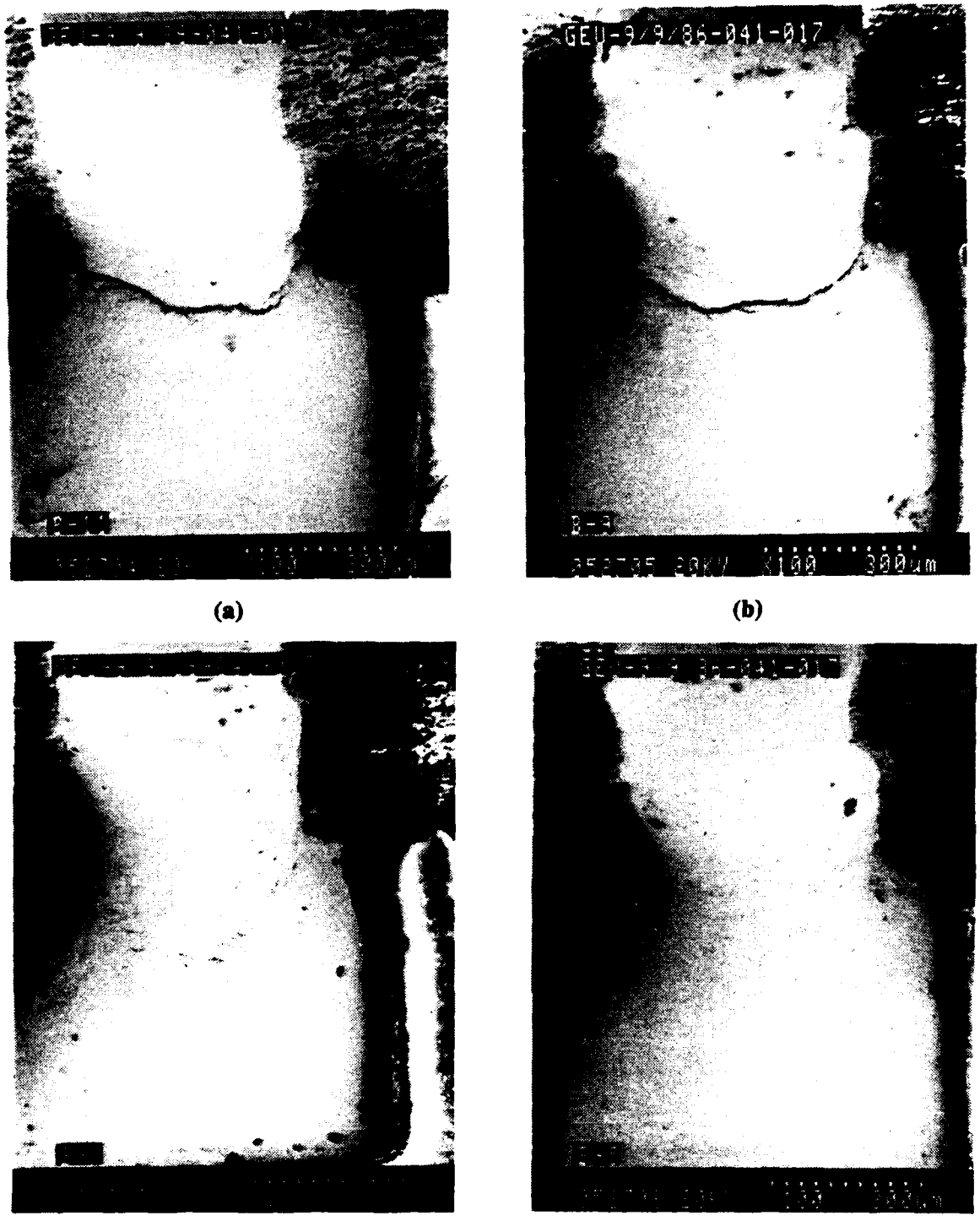

Figure 10. **Fillets of joints cycled to a 60% drop in load. (a) Joint with a resistance increase of 0.3%, (b) joint with a resistance increase of 0.15%, (c) joint with a resistance increase of 0.12%, and (d) joint with a resistance increase of 0.11%.**

very fine cracks. The resistance increase was 0.12% and 0.11%, respectively.

Figure 11 shows joints cycled to a load drop of 74%. The joint in Figure 11a exhibited a resistance increase of 0.54%, and a large crack is visible. The joint in Figure 11b exhibited a finer crack and a resistance increase of 0.19%. No crack is visible in Figure 11c, and the resistance increase was only 0.03%. As a general rule, when the resistance increase is 0.1% or greater, a crack can be observed in the joint fillet at 50-100×. The smallest resistance increase for which a corresponding crack in the fillet was observed was 0.09%, but the crack was not completely around the fillet.

A cross-section of a typical crack which goes completely through a joint is shown in Figure 12. The crack runs under the chip carrier, into the fillet, and through the fillet at about 45 °. The geometry of the position of the CC and PWB pad made the crack start near the PWB. This is somewhat atypical: generally the crack under the CC runs close to the CC. This joint is also atypical because it does not contain a void.

The preceeding observations and the analysis of the stress distribution in a CC/PWB joint [11,12] explain why the rate of load drop decreases with increasing cycling (see Figure 7). The load drop behavior illustrated in Figure 7 is quite different from that observed in experiments on simple joints without fillets [2]. In those experiments, the $(1-\frac{\Delta P}{\Delta P_m})$ vs. N curves were linear, unlike the data of Figure 7. The slope, however, was a function of the applied plastic strain which was maintained constant in those experiments. The drop in load was due to the development of a fatigue crack which reduced the load bearing area [2]. That cracking took place in a nominally uniform stress field (neglecting the stress concentration ahead of the crack). In the present experiments, however, the fatigue crack growth, which also reduces the load, takes place in a highly non-linear stress and strain field [11,12]. The initial cracking takes place under the chip carrier where the stress and resulting strains are the highest. This gives rise to the initial rapid drop in load. As the crack emerges from under the chip carrier, into the fillet, it enters a nominally lower stressed region and slows down, thereby reducing the rate at which the load drops. As the crack progresses into the fillet, the stress continues to decrease, causing the rate of load drop to decrease. Thus, because of the non uniform stress field in which the fatigue crack is growing, a decreasing rate of load drop is to be expected.

The reduction in load bearing area, resulting from the fatigue crack propagation, also increases the resistance of the joint. The shape of the resistance increase curve is, however, the inverse of the load drop curve; i.e., the rate of resistance increase increases with cycling, while the rate of load drop decreases. The following simple model explains why this is so. The resistance increase comes about because the crack locally alters the current flow, which contributes to an overall increase in resistance. This can be seen by considering the total current path as a system of series resistors

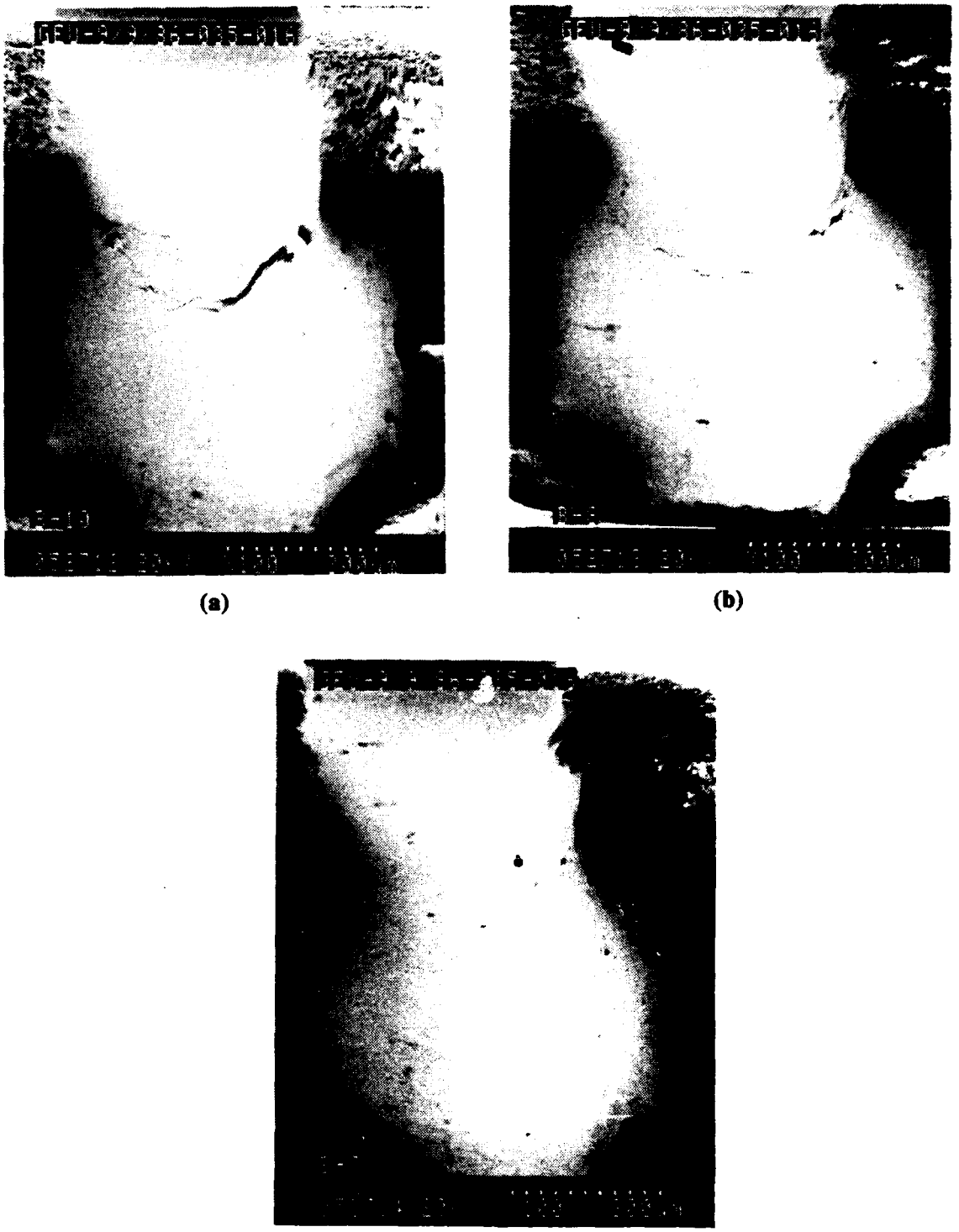

Figure 11. **Fillets of joints cycled to a 74% drop in load. (a) Joint with a resistance increase of 0.54%, (b) joint with a resistance increase of 0.19%, and (c) joint with a resistance increase of 0.03%.**

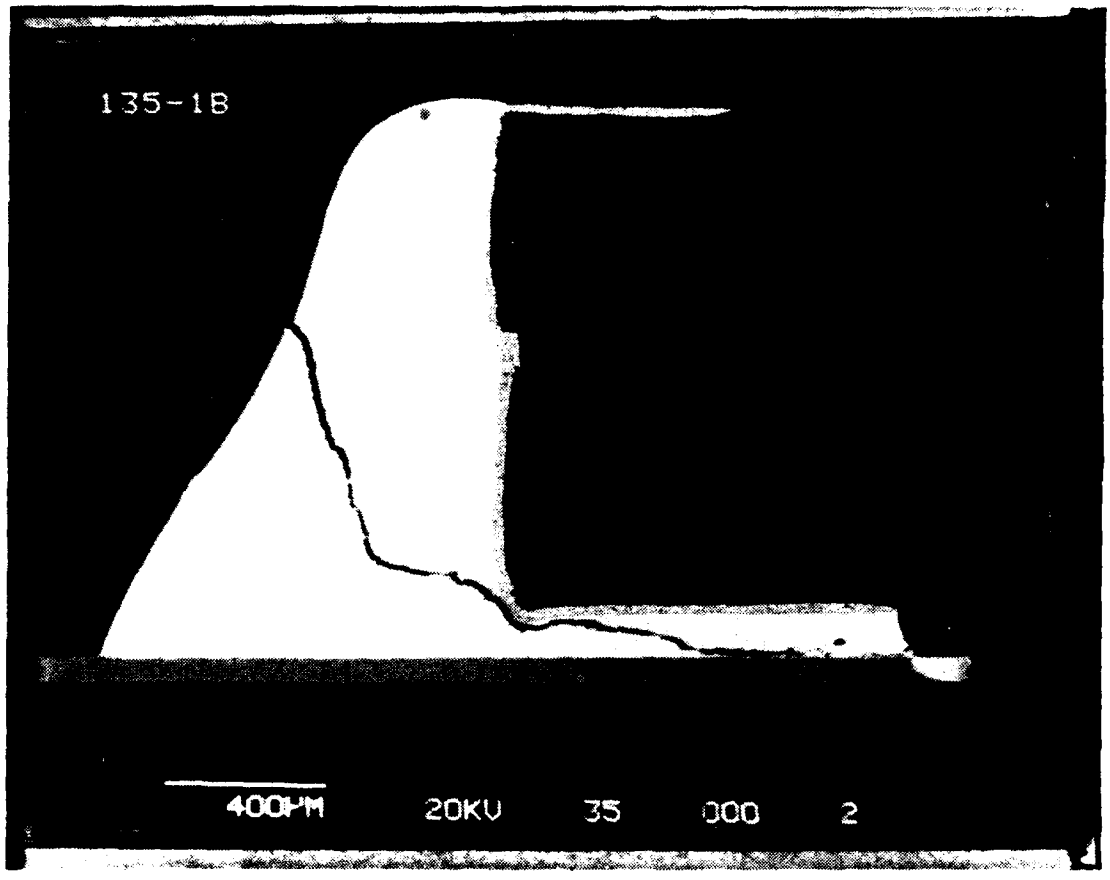

Figure 12 **Cross-section of a joint showing crack which goes completely through the joint.**

for which

$$R_i = \rho \frac{L_i}{A_i} \qquad [3]$$

where R_i is the resistance of the ith resistor of length L_i and area A_i. The overall resistance R is

$$R = \Sigma R_i \qquad [4]$$

The influence of cracking on the resistance increase can be seen more clearly by considering the following simple example. Consider a simple cylinder of length L_o and an area A_o whose resistivity is ρ. The resistance, R_o , is thus

$$R_o = \rho \frac{L_o}{A_o}. \qquad [5]$$

Now, suppose that a crack (illustrated in Figure 13) is made in the cylinder such that the *uncracked* area at the crack is A_c and the cylinder is divided into three regions of length L_1 , L_2 , and L_c (the thickness of the crack). The resistance is now

$$R = \rho\left(\frac{L_1}{A_o} + \frac{L_2}{A_o} + \frac{L_c}{A_c}\right). \qquad [6]$$

For $L_1 + L_2 >> L_c$ the fraction change in resistance is given by

$$\frac{\Delta R}{R_o} = \frac{L_c A_o}{L_o A_c} \qquad [7]$$

The increase in resistance depends upon the relative value of the width of the crack (separation of the crack faces) L_c to the initial length of the resistive path L_o . If the resistance was measured at the crack faces so that $L_c = L_o$, then the change in resistance would be equal to the change in the area conducting the current. The L_c/L_o terms determine the sensitivity of the resistance measurement to crack growth, which reduces A_c .

Equation 7 is plotted vs $\frac{A_o - A_c}{A_o}$, where $A_o - A_c$ is the cracked area, in Figure 14. The calculation, shown as the solid lines, was made for two values of L_c/L_o where $L_c/L_o << 1$.

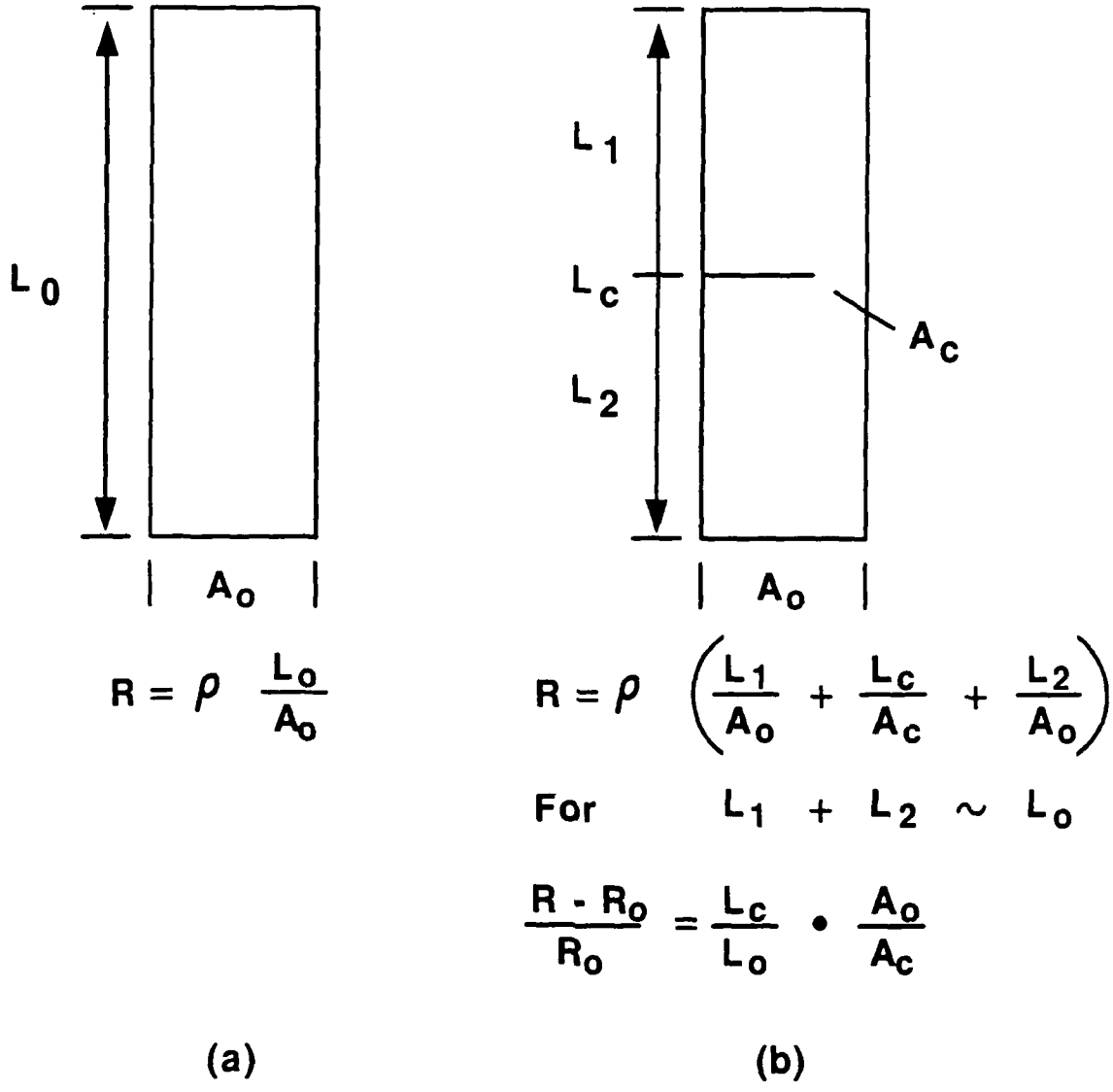

Figure 13. **Resistance of a cylinder. (a) Without a crack and (b) with a crack of thickness L_c which locally reduces the current carrying area to A_c.**

Assuming no cyclic hardening or softening, i.e., the flow stress remains constant, then

$$\frac{\Delta P_m}{A_o} = \frac{\Delta P}{A_c} \qquad [8]$$

or

$$\frac{A_c}{A_o} = \frac{\Delta P}{\Delta P_m} \qquad [9]$$

where ΔP_m is the maximum hysteresis load range which occurs at A_o and ΔP is the hysteresis load range when the area is A_c. Thus, $\frac{A_o - A_c}{A_o} = \frac{\Delta P_m - \Delta P}{\Delta P_m}$, so Figure 14 also displays R/R_o vs. $\frac{\Delta P_m - \Delta P}{\Delta P_m}$. The dotted curves show the measured R/R_o (corrected for the very small changes in the dummy resistance) vs. the measured values of $\frac{\Delta P_m - \Delta P}{\Delta P_m}$ (see Figure 7).

The data plotted in Figure 14 was taken from the same specimen whose hysteresis loops are shown in Figure 6, resistance measurements listed in Tables 1 and 2, and load drop and resistance increase displayed in Figure 7. The data for three joints is shown in Figure 14, which presents the data for the joint showing the largest resistance increase, the median joint (i.e., the joint showing the sixth largest increase out of the eleven joints on the row where failure occurred), and the joint showing the smallest resistance increase. The median and minimum joints agree roughly with the $L_c/L_o = 2\times10^{-4}$ curve. Unfortunately, this test was stopped at only about 80% load drop because of the large resistance increase of the maximum joint. Figures 15 and 16 show the results of tests continued to over a 90% drop in load. As can be seen, the median curve agrees reasonably with the $L_c/L_o = 2\times10^{-4}$ curve. This should not be surprising. The load drop data reflects the average of the behavior of the individual joints, thus it should correlate better with the median joint than the max or min joints. The L_c/L_o value of 2×10^{-4} is also reasonable. L_c is on the order of 1×10^{-4} in. (2.5×10^{-3} mm). L_o includes not only the length of the solder joint (about 0.05 in. (1.27 mm)) but also the effective length of the circuit path through the chip carrier (which is on the order of 0.5 in. (12.7 mm) to account for the higher resistivity of the metallized path compared to that of the solder joint). L_o is thus on the order of 0.5 in. (12.7 mm). This makes L_c/L_o about 2×10^{-4}.

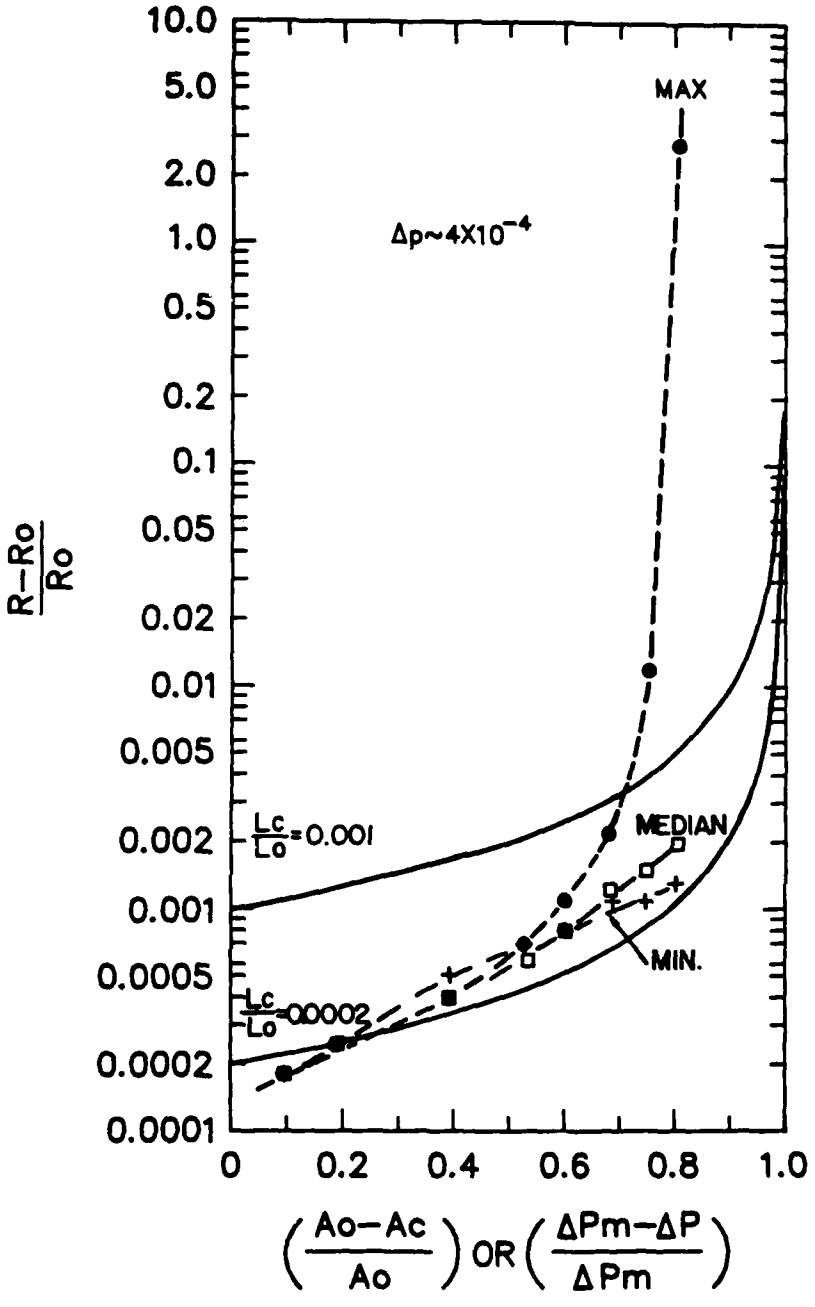

Figure 14. Resistance increase $\Delta R/R_o$ vs. the local decrease in current carrying area $\left(\frac{A_o-A_c}{A_o}\right)$ or the load drop $\left(\frac{\Delta P_m-\Delta P}{\Delta} P_m\right)$ for a test with $\Delta_p \approx 4\times10^{-4}$ in.

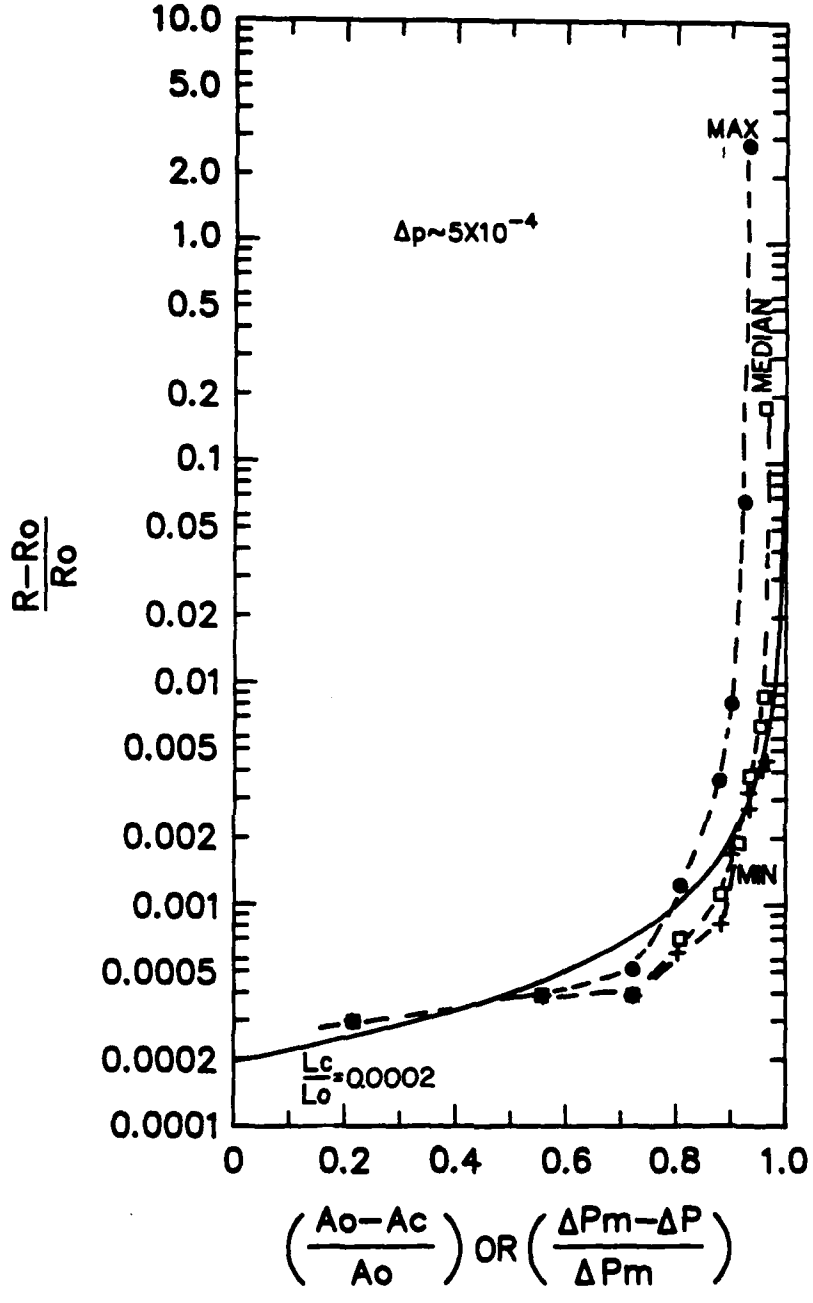

Figure 15. **Resistance increase vs. area and load drop for a test with $\Delta_p \approx 5\times10^{-4}$ in.**

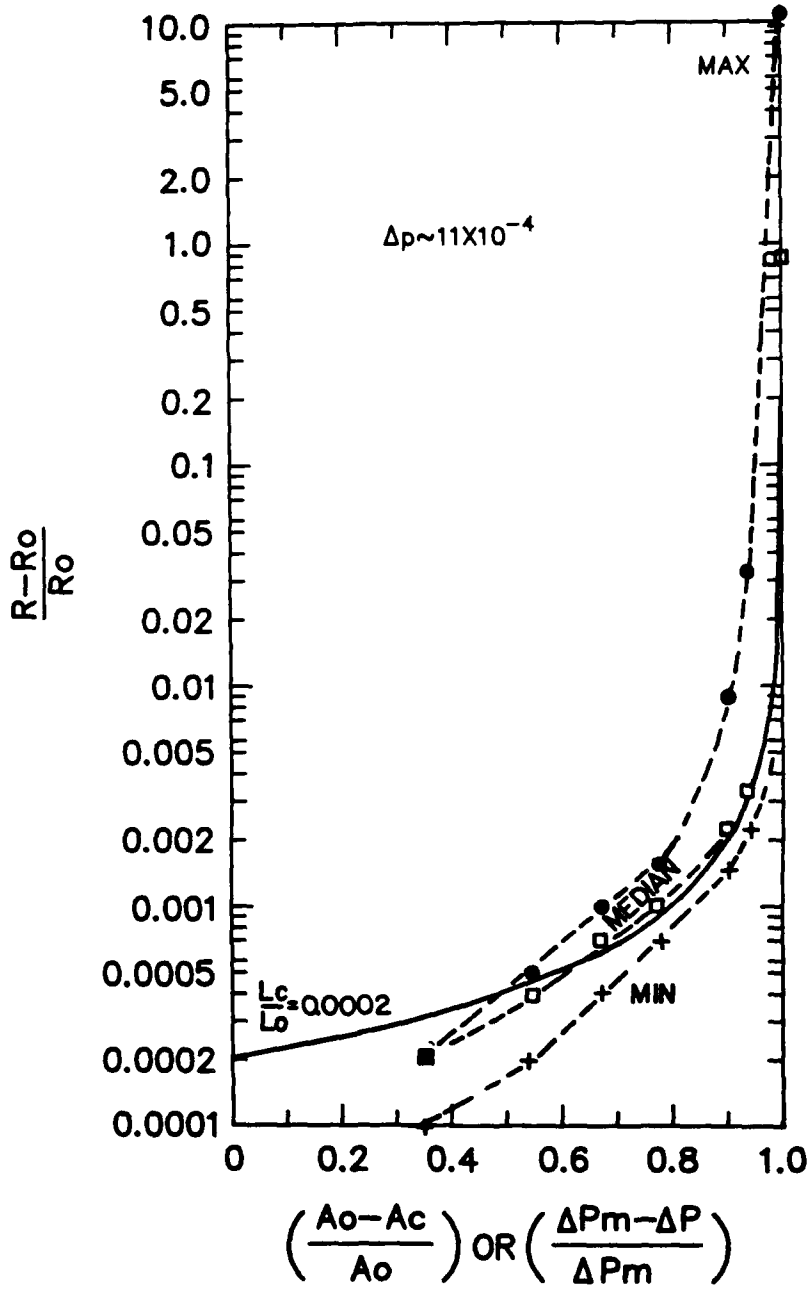

Figure 16. Resistance increase vs. area and load drop for a test with $\Delta_p \approx 11 \times 10^{-4}$ in.

While the max resistance change curves generally do correlate well with the load drop data, they are nonetheless very significant. It is the first open circuit which causes failure of the device, and thus its behavior is more important than the behavior of the median joint.

The load drop data, resistance increase data, and the observations of fatigue cracks allow the development of the picture, shown in Figure 17, which describes the sequence of joint failure. The microscopy and the initial load drop data point to initial cracking under the chip carrier at a load drop of about 25%. This is supported by the uniform, but high, stresses developed under most of the chip carrier and the initial linear behavior of the load drop curve shown in Figure 7. Figures 14-16 show that for the max., median, and min. joints, the resistance increase for a 25% load drop is about 0.02%. The 50% load drop is caused by cracks which enter the fillet. The load drop begins to slow down because of the decreasing stress. The resistance increase is on the order of 0.05%. It is only with further crack propagation that a major spread develops between the joint which shows the maximum increase in resistance and the other joints. A resistance increase of 0.1% is observed with load drops of 60-90%. By a 90% load drop, the resistance increase of most of the joints exceeds 0.1% (the average median joint increase is 0.2%) and cracks are visible in the joints. At this level of fatigue, the resistance increase of the most fatigued joint is generally 1% or greater (some may even show an open circuit) and a very large crack is visible.

While a crack may be visible through the fillet, there may still be some passage of current through the crack faces where they touch. Also, while a crack may reach the surface of a fillet, there may be internal regions which are not cracked and still pass an electrical current. Thus, even though a crack is visible in the fillet, the resistance increase may be as small as 0.1%. With more cycling, however, the resistance continues to increase until an open circuit is made. In general, it takes a load drop of about 90% before the first open circuit is reached and more than a 95% drop in load before all the joints exhibit open circuits.

3.2 Influence of Bending

The final test configuration that was developed tested the solder joints without applying any appreciable bending movements. The earliest test configuration that was used did, however, apply a small but measurable bending movement, so before we go into the data in more detail, it is necessary to determine the extent to which this bending influenced the results. In these early tests, the joints were located 0.35 in. from the load line. At the maximum applied load of 100 lb, this caused a 35 in/lb bending movement. The bending movement produced a 5×10^{-4} deg/lb bend compliance or 2.5×10^{-4} deg/lb for each row of joints.

Figure 18 shows the fatigue life N_f defined as the number of cycles to reduce the load in half, as a function of the applied displacement Δ_p . This displacement was

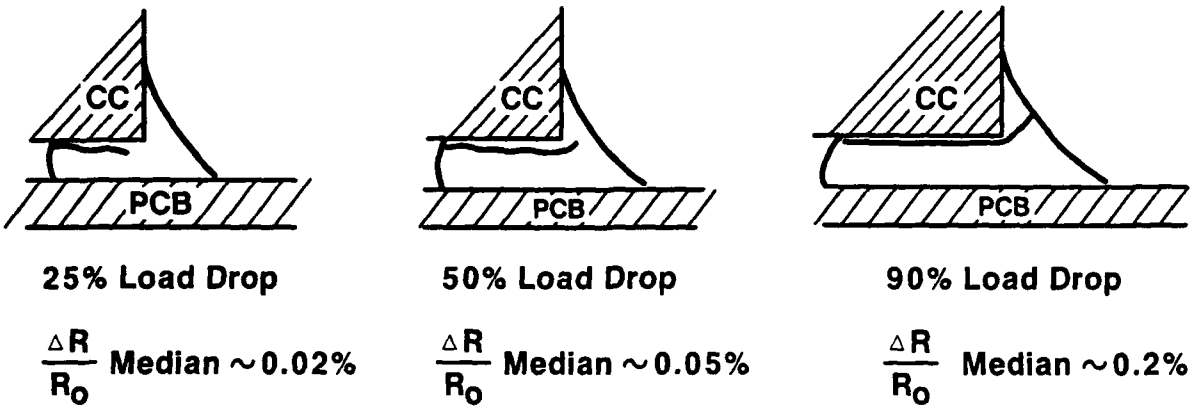

Figure 17. Sequence of CC/PWB joint failure.

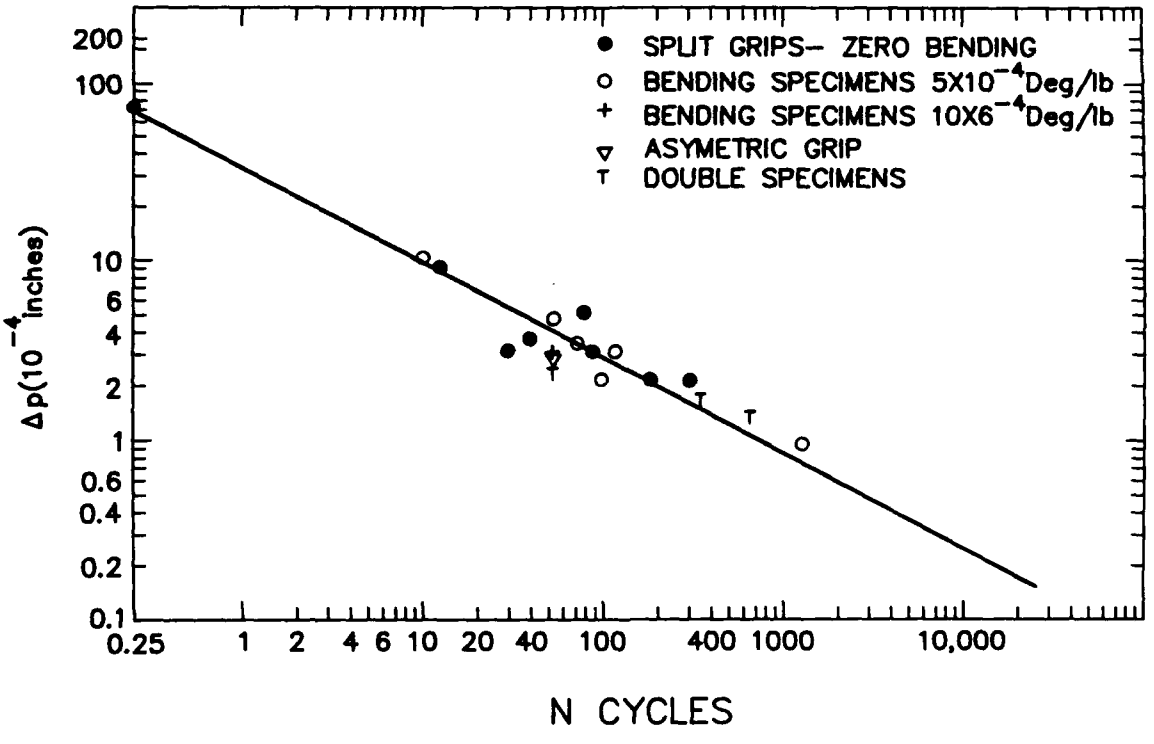

Figure 18. Fatigue life for a 50% drop in load correlated with the degree of bending applied to the joint.

measured across both rows of joints. The data points are denoted by o, •, +, ∇ or T, depending on the nature of the tests. The tests denoted by the • were performed utilizing the final arrangement consisting of split grips with the joints at the load line (described in the procedures section). The o points were taken with the early arrangement which applied the 5×10^{-4} deg/lb bending. The ∇ point was taken with a special grip which placed the joint at the load line but applied the load asymetrically (with a 0.35 in/lb bending movement). This reduced the bending movement. The + point was taken with these grips reversed. This placed the specimen 0.70 in. from the load line, doubling the bending to produce 10×10^{-4} deg/lb. Lastly, the *T* points were taken in three preliminary tests which utilized a test configuration which allowed two specimens to be tested at one time. Here, the bending movements induced in each specimen canceled, so there was no net bending of the joints. Figure 18 shows that the degree of bending, at least up to 10×10^{-4} deg/lb, did not influence N_f.

In subsequent Figures, the exact nature of the test setup and degree of bending will not be discussed. In all, 16 tests were performed and discussed here. Eight utilized the split grip and eight utilized other grip arrangements. The three tests run with double specimens are not discussed further because of control problems that were created when large cracks developed. *No difference in the Δ_p vs. N_f correlation is noted if only the eight split grip, zero bending movement specimens are used for the correlation.*

The final test configuration which utilized the split grip was adopted not only because it eliminated the bending, but also because it allowed the attachment of the yoke (see Figures 4 and 5) and the measurement of the displacement of the individual row of joints.

3.3 Coffin-Manson Low Cycle Fatigue Behavior; Load Drop Data

There are many possible definitions of fatigue failure. The drop in load and increase in resistance can both be used to define failure with various load drop and resistance increase criteria. Several different criteria can also be used to define the displacement, which causes the failure, as illustrated in Figure 19. The displacement measured across each single row of joints (denoted top and bottom because of their position in the test machine) is recorded, as is the sum of these displacements. The plastic strain computer was set up to determine the plastic strain for the sum of the T + B rows. This plastic strain, as measured at the cross head reversal, is denoted as Δ_p (see Figure 19). Since the plastic strain computer was not set up for each row of joints individually, plastic strain hysteresis loops were not drawn for the displacements from the individual row of joints. The plastic displacement was, therefore, measured for each single row from the hysteresis loop width at zero load and is denoted as Δ_{ps}. The single displacement data utililzed in the subsequent tests is for the row of joints which showed the greatest degree of cracking. In the case of the data shown in Figure 19, it was the bottom row of joints (i.e., $\Delta_{ps} = \Delta_B$ which is the row of joints which

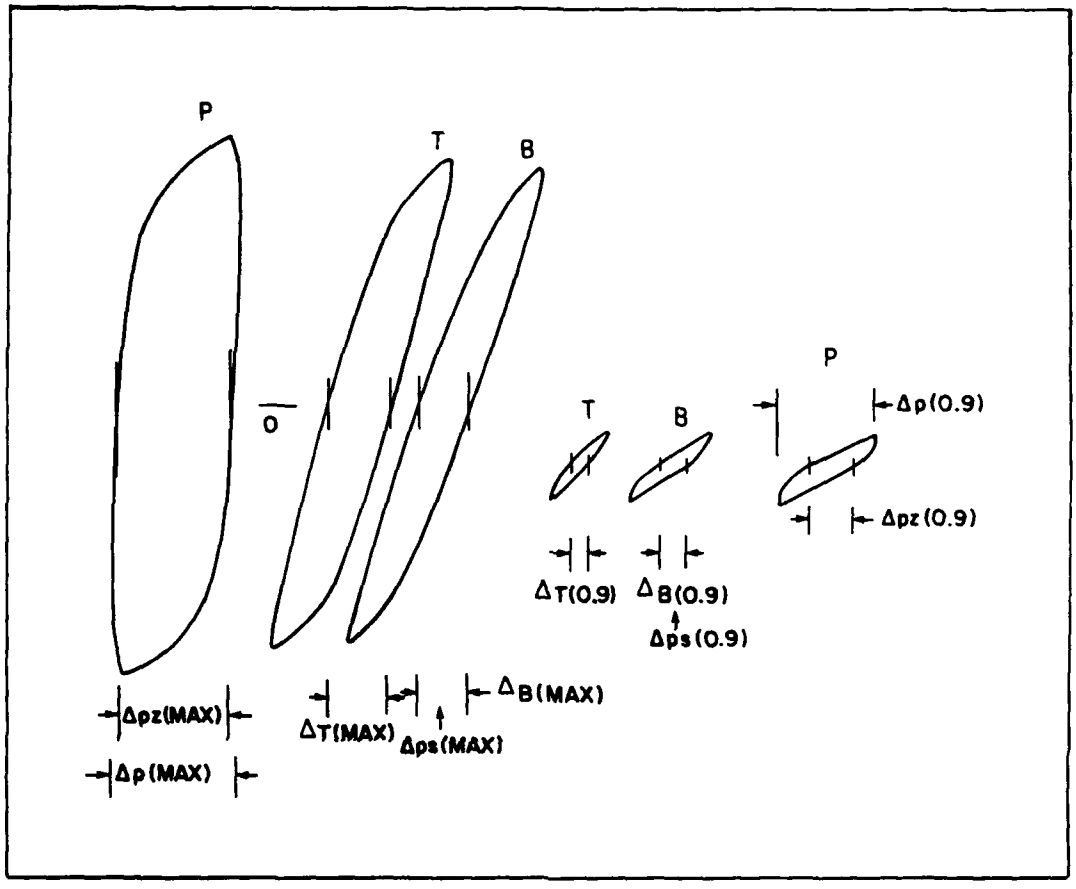

Figure 19. Hysteresis loops and the definitions of different displacements.

showed the most cracking).

The hysteresis loop width was also recorded at zero load for the sum of the top and bottom row displacements. It is denoted as Δ_{pz} , and will be discussed later. The distinction between the plastic displacement for each row and the sum of these displacements was made because it provides information on how the applied displacement is partitioned between the top and bottom rows of joints and how this influences the fatigue process.

The fatigue life N_f is related to the applied plastic strain by the well known Coffin-Manson Law [13-18] which has been shown to apply to solder fatigue [2-5]. In these current tests, a known displacement is applied to the joints. This can be converted into a strain by dividing by an appropriate length. Unfortunately, the complex geometry of the solder joint means that a severe strain gradient develops as the result of the application of a fixed displacement and only a rather complex analysis can be used to convert this displacement with a strain distribution. Rather than deal with the strain-life behavior, Figure 18 and the subsequent figures relate the fatigue life N_f with an applied displacement, Δ_p , according to a pseudo Coffin-Manson Law, i.e.,

$$N_f^{\alpha} \Delta_p = \theta \qquad [10]$$

Figures 20-30 show the fatigue life, N_f, as defined by various decreases in the load range. All conform to this pseudo Coffin-Manson Law. The different failure criteria are used because they provide information about the mechanism of joint failure. Fatigue is defined by increases in resistance also provide important information, but will be discussed separately in a subsequent section.

Figure 20 shows the number of cycles, N_f, to reduce the load by 25% vs. the sum of the plastic displacement of both rows. This displacement, denoted as $\Delta_p(max)$, was measured at the cycle where the maximum load is reached. This generally was the first cycle, although in a few cases, the maximum load was reached on the second or third cycle. (There is an interplay between some cyclic hardening which raises the load and cracking which reduces it).

As has already been discussed, the 25% load drop criteria for failure defines an early stage in life where the fatigue cracking is confined to the solder beneath the chip carrier. The 70% confidence band, shown on figures 20-29, defines a 70% probability that if another test were run, the data would fall within the band. It is close to a plus or minus one standard deviation band, but not exactly equal to it. This 70% confidence band was employed because this data was used as a reference for other experiments not discussed here.

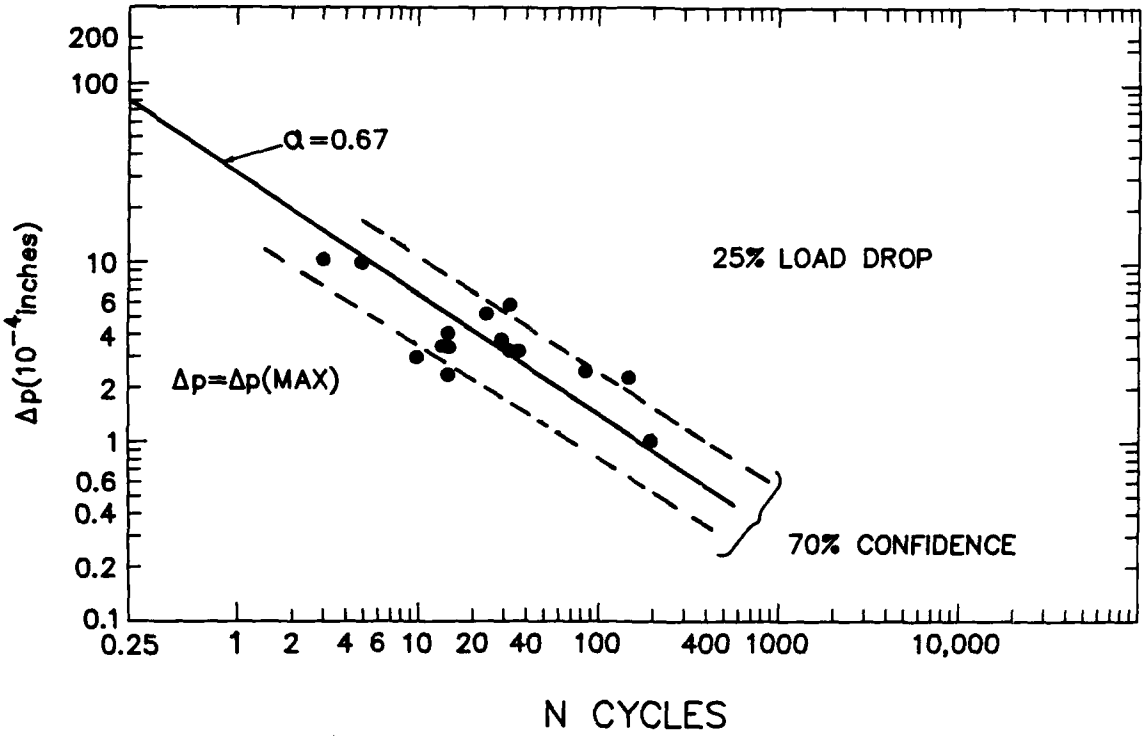

Figure 20. **Displacement (sum across both rows of joints) vs. fatigue life for a 25% drop in load.**

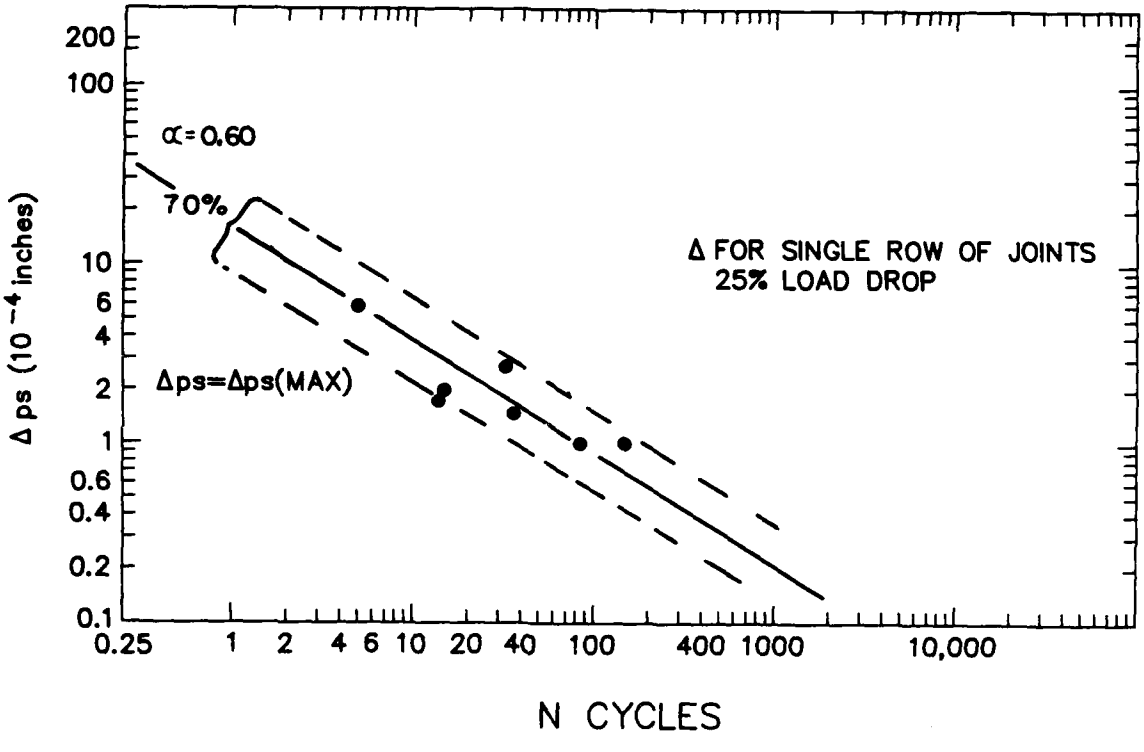

Figure 21. **Displacement of a single row of joints vs. fatigue life for a 25% drop in load.**

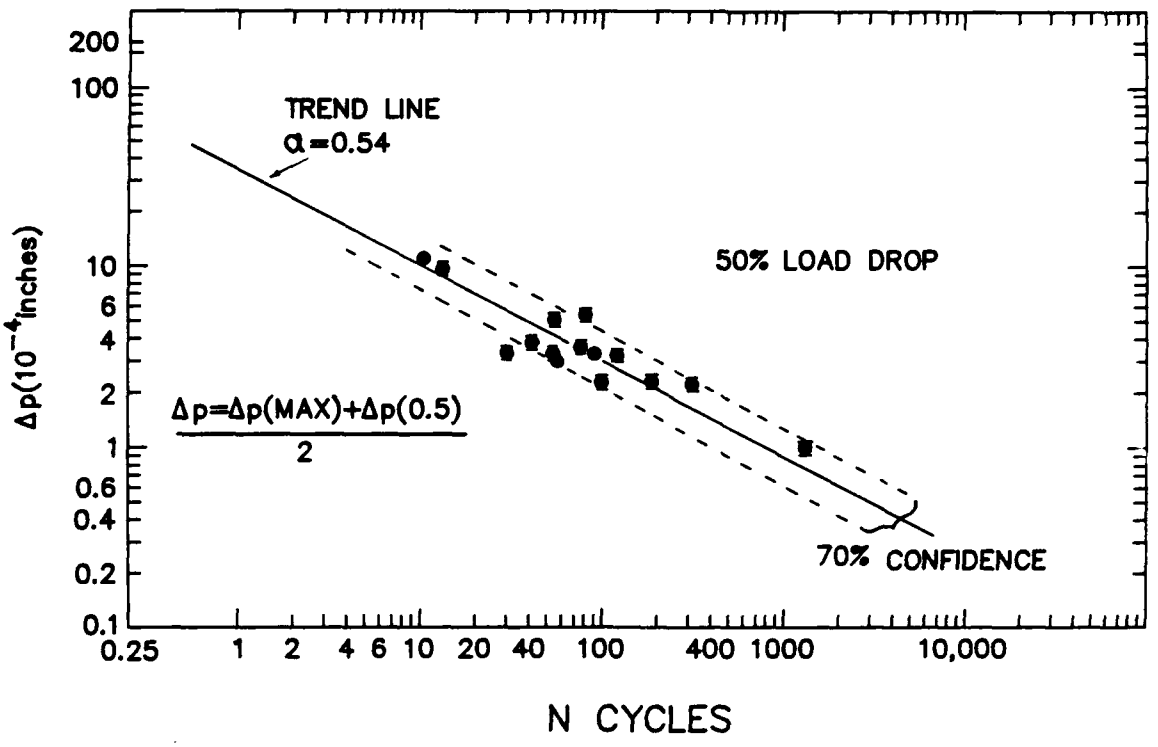

Figure 22. **Displacement (sum across both rows of joints) vs. fatigue life for a 50% drop in load.**

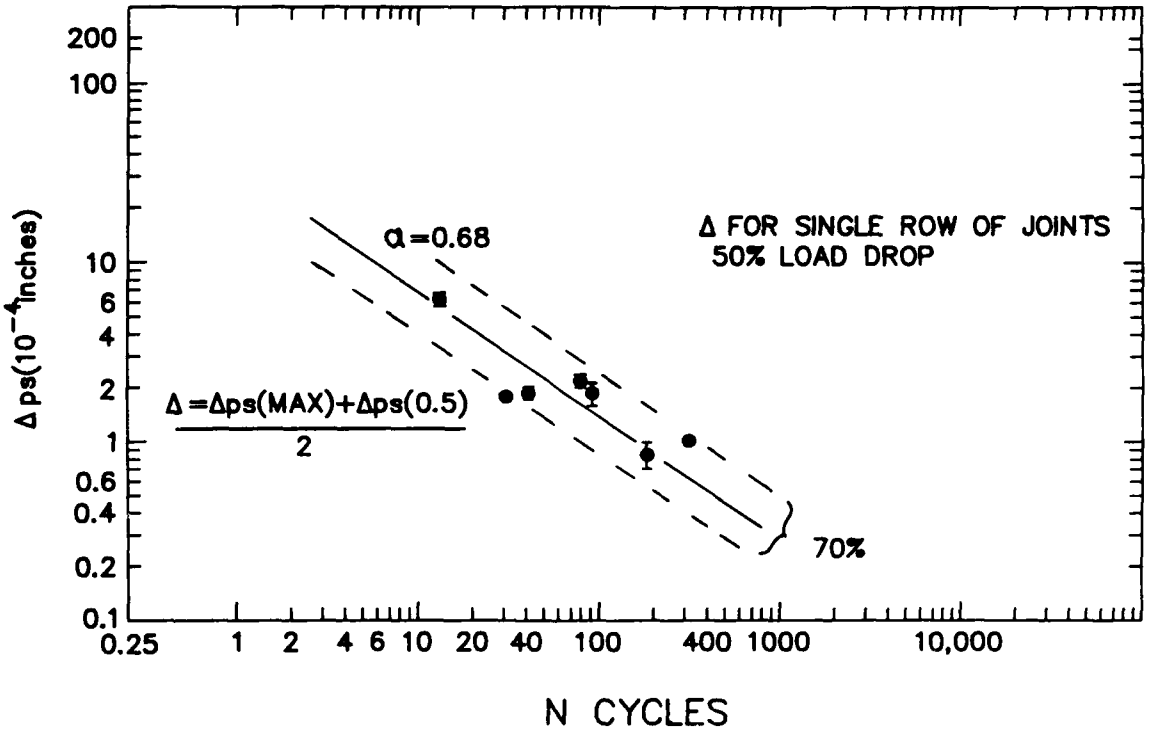

Figure 23. **Displacement of a single row of joints vs. fatigue life for a 50% drop in load.**

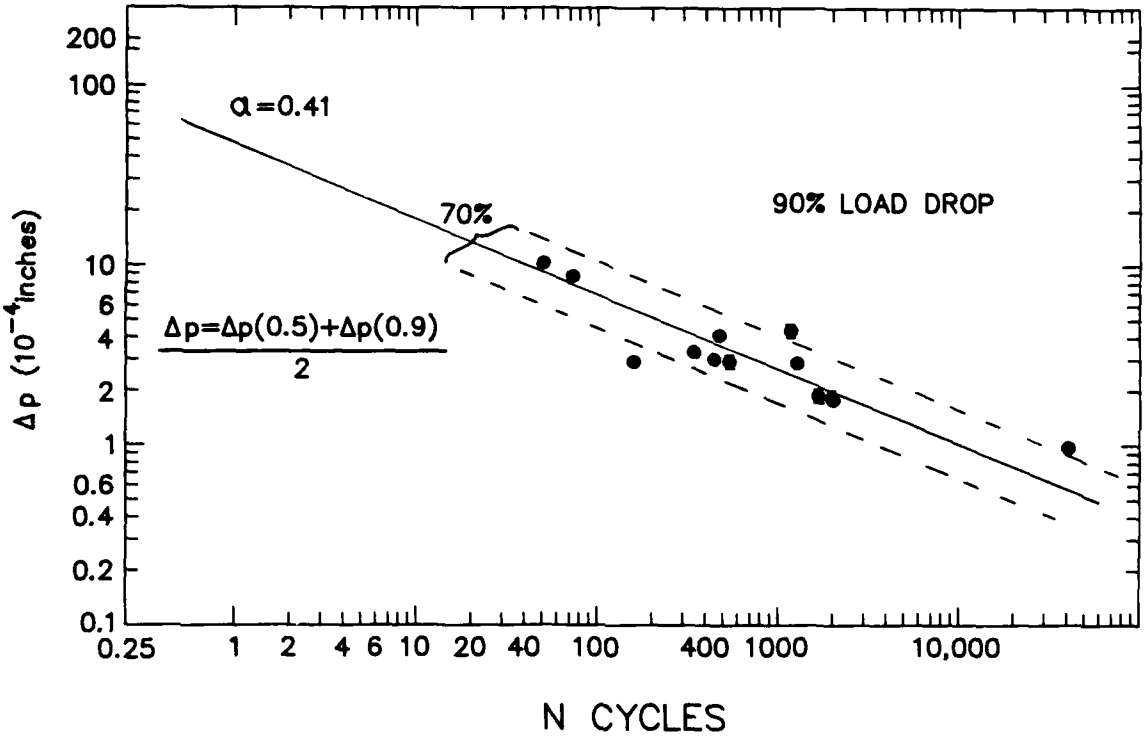

Figure 24. **Displacement (sum across both rows of joints) vs. fatigue life for a 90% drop in load.**

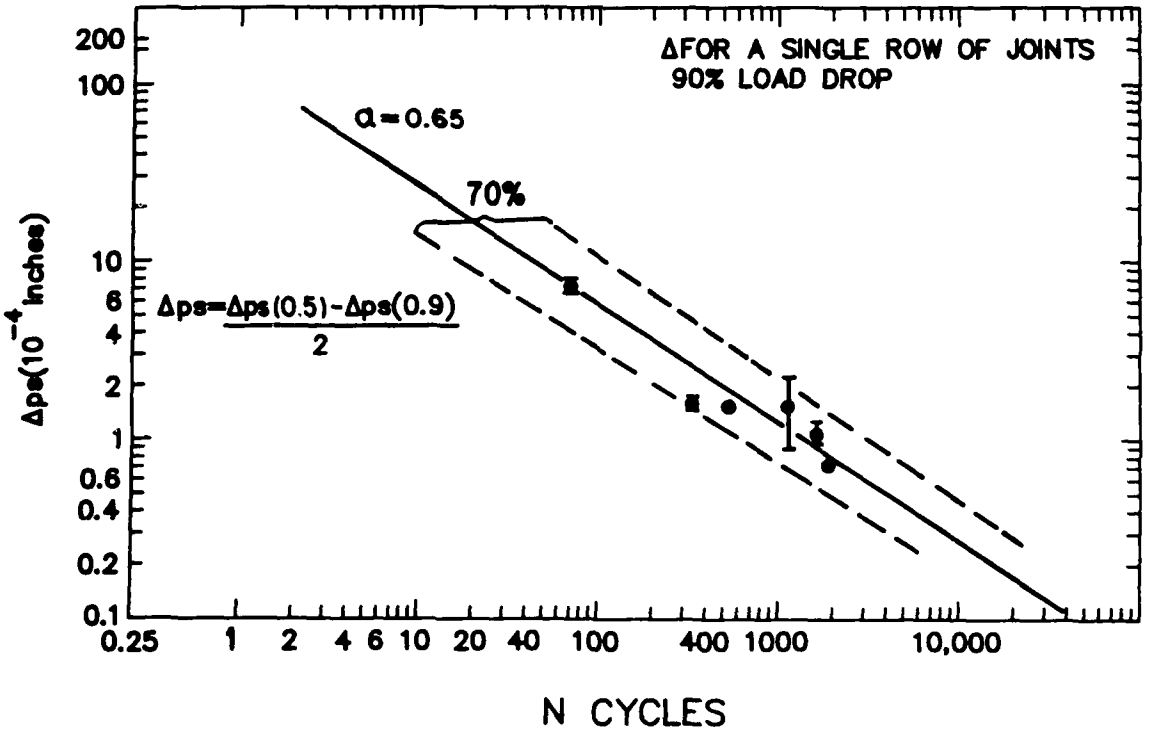

Figure 25. **Displacement of a single row of joints vs. fatigue life for a 90% drop in load.**

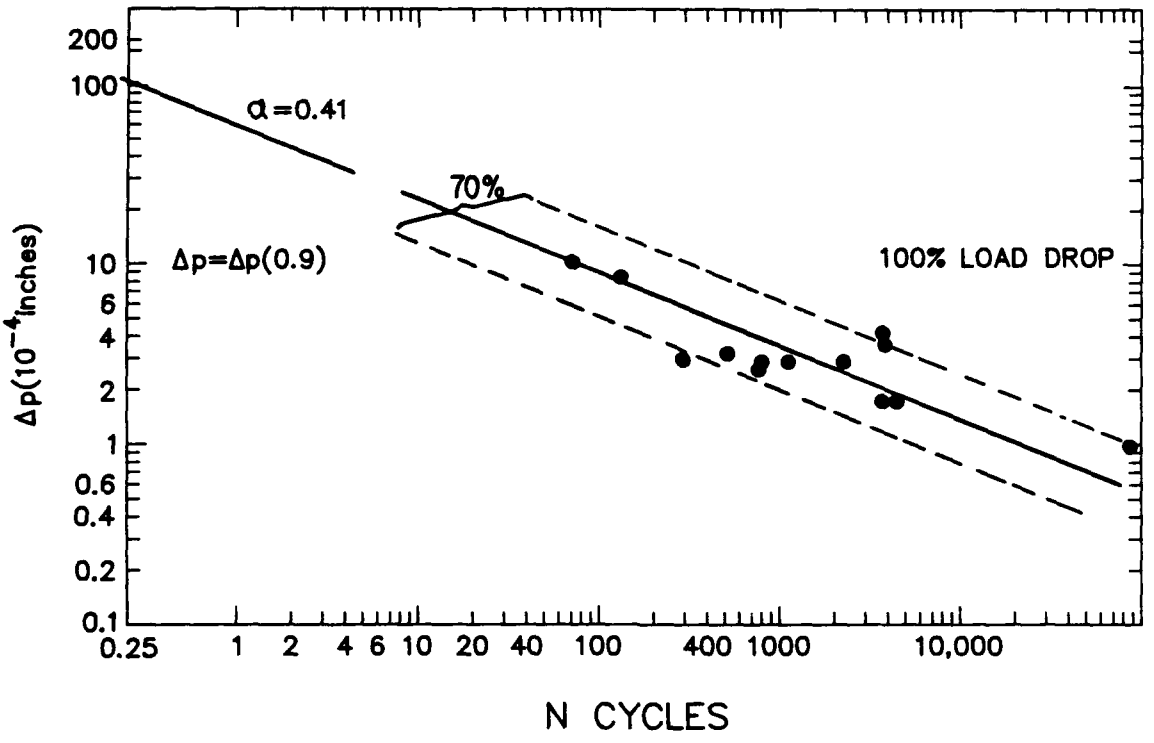

Figure 26. **Displacement (sum across both rows of joints) vs. fatigue life extrapolated to a 100% drop in load.**

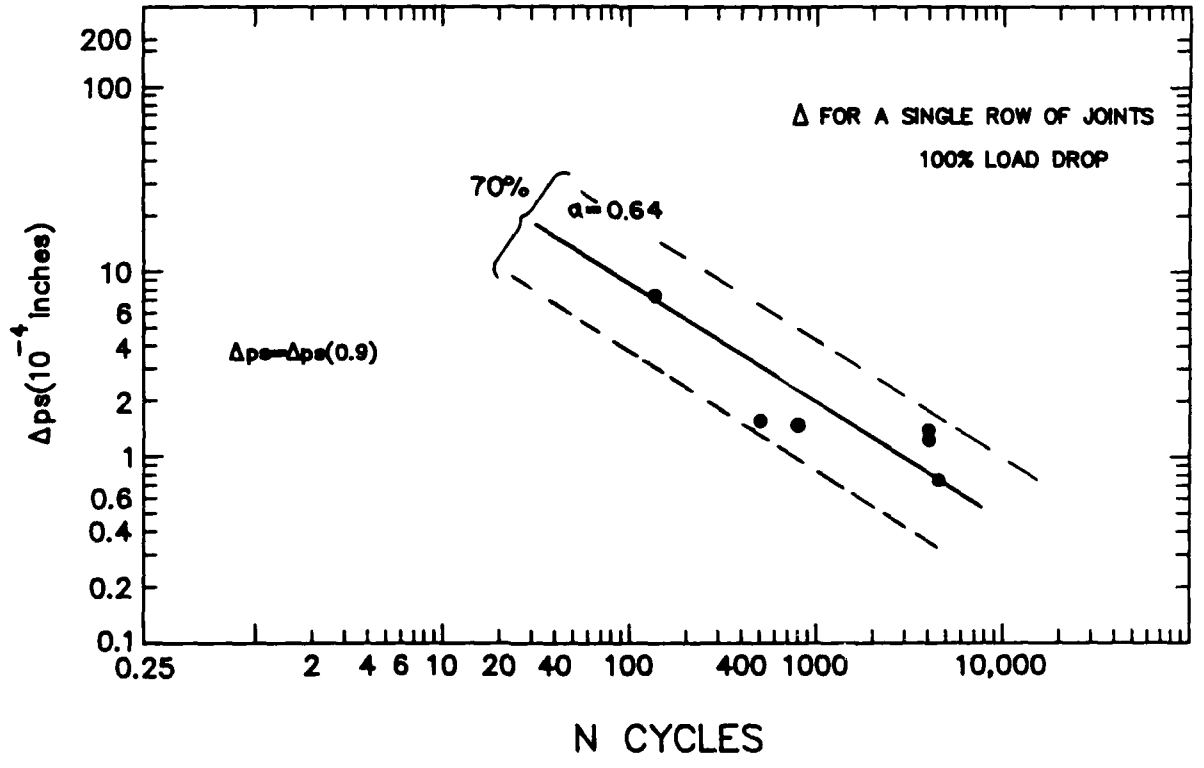

Figure 27. **Displacement of a single row of joints vs. fatigue life extrapolated to a 100% drop in load.**

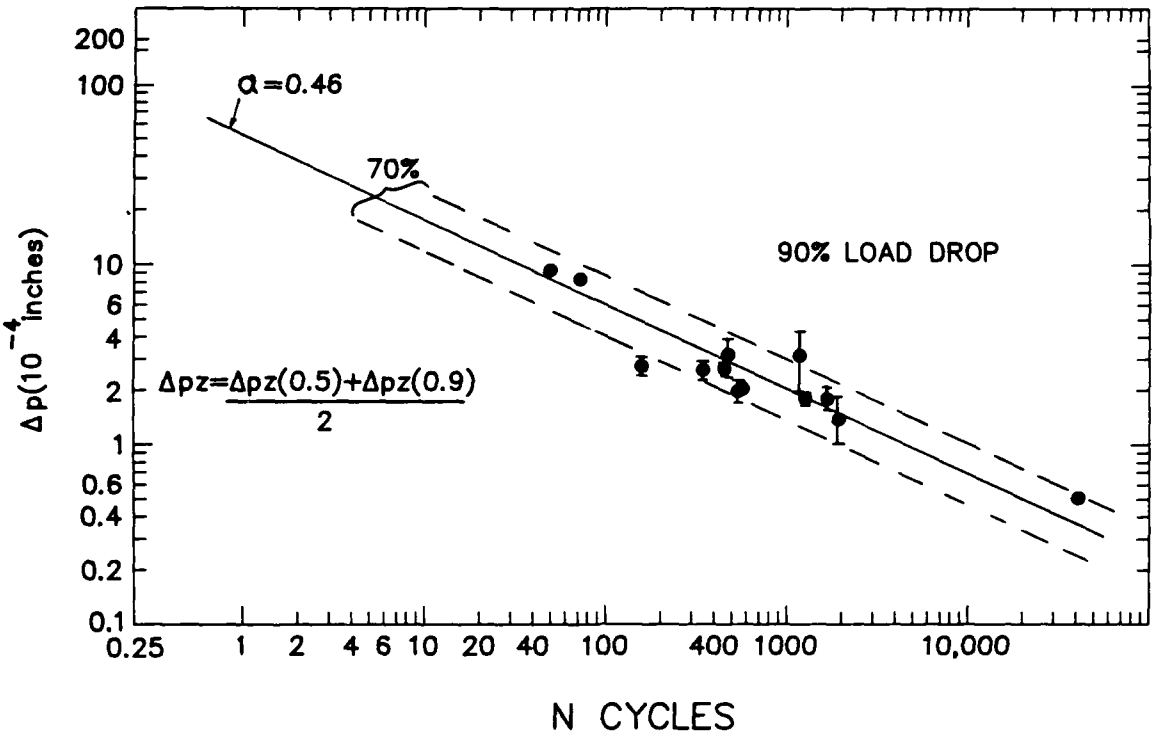

Figure 28. **Displacement measured at zero load for a 90% drop in load. The displacement is the sum of that measured across both rows of joints.**

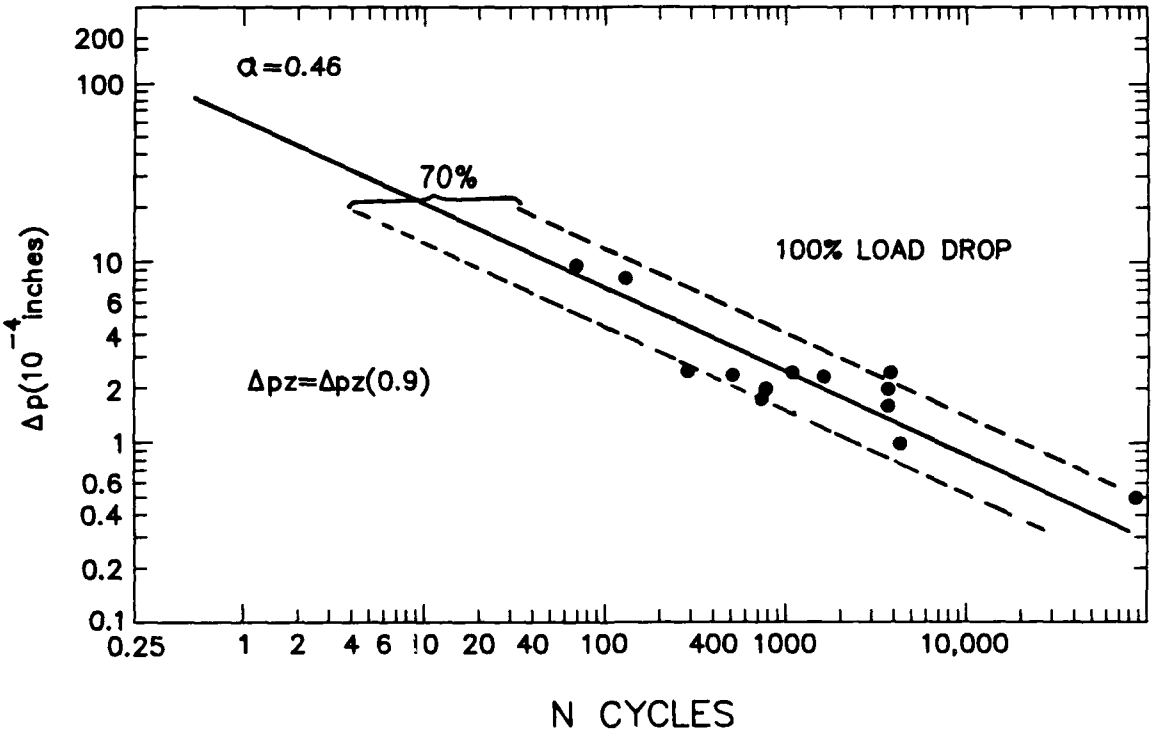

Figure 29. **Displacement measured at zero load extrapolated to a 100% drop in load. The displacement is the sum of that measured across both rows of joints.**

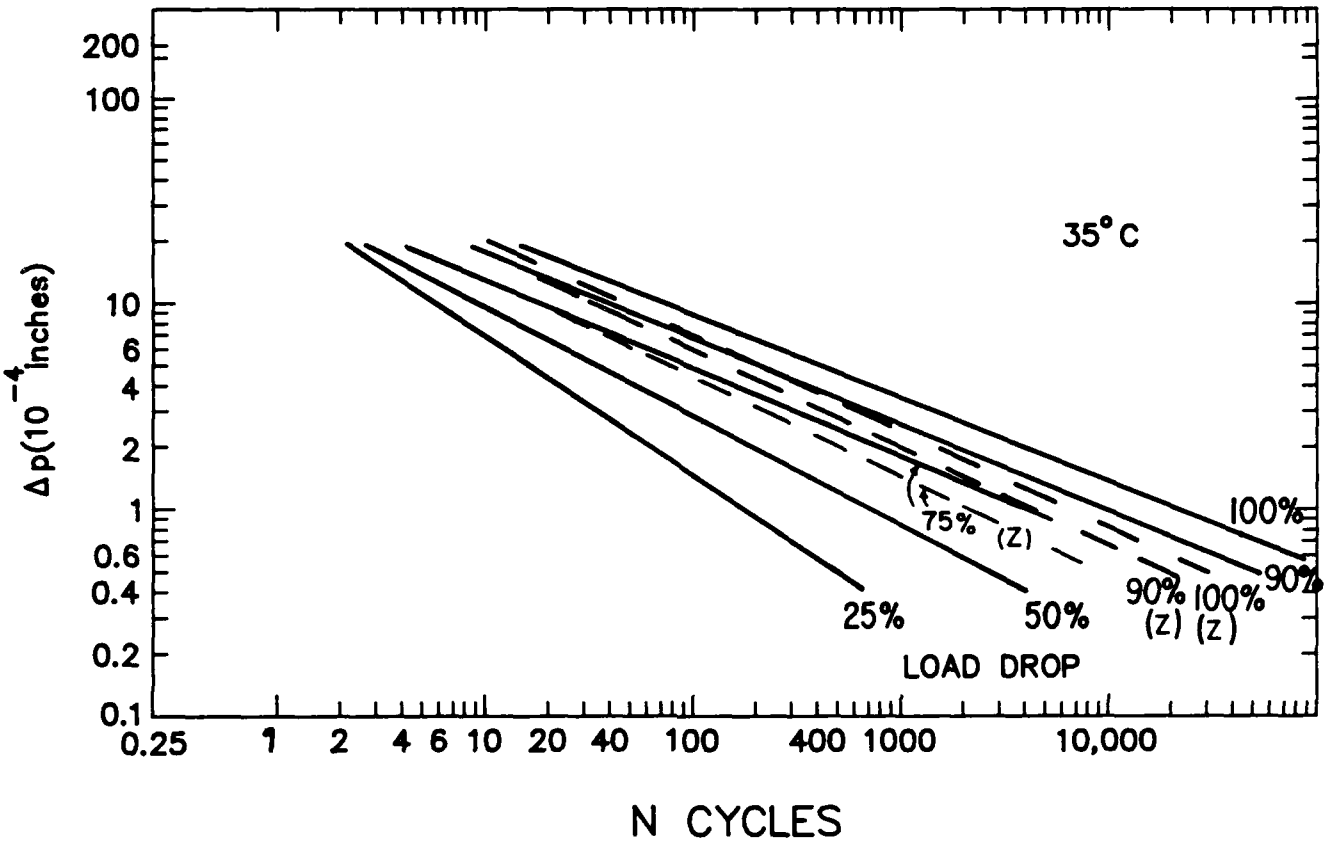

Figure 30. **Summary of the displacement (sum across both rows of joints) vs. the fatigue life measured at 25, 50, 75, 90 and 100% drops in load.**

In addition to the fatigue data, Figure 20 (and equivalent subsequent figures) also shows the results of a tensile test which is equivalent to a fatigue test with $N_f = 1/4$ cycle. The data point at $N_f = 1/4$ is the monotonic strain required to reduce the load by 25% in the tensile tests. In subsequent tests, where 50%, 90%, and 100% drops in load are used as the failure criteria, the $N_f = 1/4$ strain is that required to reduce the load in the tensile test to 50%, 90%, and 100% of its maximum value.

Figure 21 shows the failure, defined by a 25% drop in load, correlated by the displacement $\Delta_{ps\,(max)}$ measured across a single row of joints. The measurement was made for a hysteresis loop taken as close as possible to the maximum load hysteresis loop. Since only one xy recorder was used, the hysteresis loops for each type of displacement (i.e., top, bottom, top + bottom total displacement) were not drawn for every cycle.

There are fewer data points than for the data of Figure 20 because in the early tests only a single extensometer was used across both rows of joints instead of one for each row. Thus, there are about twice as many data points for the Δ_p measurements of the plastic displacement across both rows compared to the Δ_{ps} measurements of single rows. Restricting the data to only those tests run with two extensometers does *not* change the data correlations. The Δ_{ps} plotted in Figure 21 and other figures which use this parameter was the displacement measured at the row (top or bottom) at which the final failure occurred, or where the most joints showed a rise in resistance.

If the displacement is evenly partitioned between the two rows of joints, then Δ_{ps}/Δ_{pz} should be equal to 0.5, and this is approximately the case. At the start of the test, Δ_{ps}/Δ_{pz} was found to be 0.49 ± 0.07, with a minimum value of 0.42 and a maximum of 0.61. (The displacement Δ_{pz} is used rather than Δ_p because Δ_{ps} is measured at zero load but Δ_p is not).

As the crack propagates and reduces the load bearing area, it reduces the amount of load required to produce Δ_{ps} . The load is also reduced in the other row of joints, reducing the displacement developed across this row and the resulting fatigue failure in these joints. Since the control is on the sum of the displacements across both rows as the displacement decreases in one row, it increases in the other. By a 50% drop in load Δ_{ps}/Δ_{pz} increases to 0.56 ± 0.12. The displacement Δ_{ps} is measured across the row of joints in which failure occurs and the displacement is concentrated, hence the increase in Δ_{ps}/Δ_{pz}. By a 90% drop in load, Δ_{ps}/Δ_{pz} increases to 0.75 ± 0.14.

There is some variation in Δ_{ps}/Δ_{pz} because there is a variation in the degree to which cracking begins on one row of joints or the other. If the cracking develops in both rows to an equal degree, then there will be little or no increase in Δ_{ps}/Δ_{pz} and cracks are noted in both the top and bottom rows of joints. Cracking occurred in both rows of joints in 5 (out of 16) tests, but even here there was more cracking in one row

than the other. In general, cracking began first in one row. The shift in displacement then retards or prevents cracking in the other row (i.e., no cracks were observed and no resistance was noted). This shift in displacement explains why the failures occur predominantly only in one row of joints, even if a weak joint is present in an otherwise stronger row. The behavior of the row of joints and the partition of the displacement appear to be dominant over the behavior of a particular joint. A weak joint in a weak row will probably start the failure process, but a weak joint in a strong row may not even crack.

Figures 22 and 23 show the fatigue behavior defined by a 50% drop in load. During the cycling to this drop in load, there was some decrease in the hysteresis loop width (due to the compliance change). The fatigue life (to drop the load in half) was therefore defined in terms of the average of $\Delta_{p\,(max)}$ and the plastic displacement at half load, $\Delta_{p\,(0.5)}$ i.e., $\frac{\left(\Delta_{p\,(max)} + \Delta_{p\,(0.5)}\right)}{2}$. The brackets define $\Delta_{p\,(max)}$ and $\Delta_{p\,(0.5)}$. Figure 22 (same as Figure 18 without the distinction as to the amount of bending) shows the results for the plastic displacement of both rows, while Figure 23 shows N_f vs. the plastic displacement of a single row of joints, i.e., for $\frac{\Delta_{ps\,(max)} + \Delta_{ps\,(0.5)}}{2}$.

The data of Figures 22 and 23 are similar to those observed with failure defined by a 25% drop in load, except that the lives are longer and the slope of the curve, α, is 0.54 for both rows compared to 0.68 for the similar 25% load drop data. The single row data shows no such decrease in α.

Figures 24 and 25 show that a similar situation occurs with the failure defined by the 90% drop in load. Here, the displacements were the average of that measured at the 50% drop in load and at the 90% drop in load, i.e., $\frac{\Delta_{p\,(0.5)} + \Delta_{p\,(0.9)}}{2}$ and $\frac{\Delta_{ps\,(0.5)} + \Delta_{ps\,(0.9)}}{2}$. This average was used rather than the average over the entire test, because most of the life is spent in the 50% to 90% load drop regime.

Figures 26 and 27 show the fatigue life extrapolated to complete failure. The total displacement observed at the 90% drop in load is used because, in going from a load drop of 90% to complete failure requires generally at least a doubling of the fatigue life; hence the 90% displacement most accurately reflects the displacement operating in this last phase of the fatigue process. Caution should be taken in using these figures because they represent an extrapolation of the data taken from about a 90% drop in load. The load drop curve is very shallow as the load drop approaches 1; hence errors are introduced in the extrapolation. As with the 50% and 90% load drop data, α is reduced for the double row of joints, compared to what was observed with the 25% load drop.

A 75% load drop correlation was also employed, but is not provided because it is very similar to the 90% and 100% load drop correlation (as opposed to the 50% load drop correlation with its larger value of α). For a 75% drop in load, the slope of the Δ_p vs. N_f curve was found to be 0.42 for both rows of joints and 0.69 with a single row of joints. The trend line for both rows of joints is shown in the summary curve, to be discussed shortly.

Some of the decrease in α that develops in the Δ_p-N_f curves is because Δ_p is not an accurate measure of the displacement. The compliance increase produces a rotation in the hysteresis loops which is not accounted for in the Δ_p measurement. The hysteresis loop width at zero load (Δ_{pz}) width at zero load more accurately reflects the plastic strain being applied, but may underestimate the strain somewhat. (If there is complete elastic unloading to zero load, the loop width at zero load gives the right strain. When reverse plastic flow begins before zero load is reached, then some of the plastic strain is neglected when the zero load loop width is used). At the start of the test, there is little difference between the zero load loop width and the loop width at the cross head reversal because the elastic unloading extends virtually to zero load. At the 50% load drop level there is a small difference between Δ_p and Δ_{pz} which gets bigger as the test progresses.

The fatigue life for 90% and 100% load drops, for the displacement defined by Δ_{pz}, is shown in Figures 28 and 29. At large displacements, the influence of the compliance increase is small because the elastic displacement is much smaller than the plastic displacement and $\Delta_{pz} \approx \Delta_p$. At small displacements, $\Delta_{pz} < \Delta_p$ and the result is to increase α when Δ_{pz} is used to define the displacement rather than Δ_p. The increase in α is, however, only from 0.41 to 0.46, so it does not explain why α is so much smaller than the α observed when a 25% drop in load is used to define failure. For this small load drop, $\Delta_{pz} \sim \Delta_p$, so there is no error introduced by using Δ_p as the definition of the displacement. The Δ_{pz} displacement was also correlated with a load drop of 75%. As with the double and single joint data discussed previously, this curve was similar to the curves for a 90% and 100% drop in load, but shifted to a shorter life. It is compared to the other zero (z) loop width curves in figure 30.

For convenience, the trend lines of Figures 20-29 and curves for a 75% drop in load are compared in Figure 30. The trend in the variation in α and the displacement of the various curves are clearly shown in this figure. A decrease in α was also observed in tests performed on single, simple joints (i.e., joints with no fillet and a large constant thickness area) [19]. It is believed that the dependence of α with the criteria used to define failure resulted from the crack growth behavior. An analysis of the theoretical shear crack growth behavior for the boundary conditions being applied showed that the crack growth rate should not increase with increasing crack length [2] as it does when tensile loading is employed. Not only does the data show no accelera-

tion in the crack growth rate, it actually shows that the crack slows down, especially at low strains (i.e., the lower the plastic strain, the greater the slowdown in the crack growth rate). This strain dependence of the slowdown in crack growth rate causes α to be dependent upon the failure criteria. The larger the load drop (i.e. crack growth) used to define failure, the greater the influence of the slowdown in crack growth rate. The current experiments are more complex than those performed on the simple joints. Here there is a slowdown in load drop (crack growth) due to the complex joint geometry (see Figure 7), and this acts in addition to any inherent slowdown due to the behavior of solder tested in shear.

The data obtained utilizing the displacement of the single row of points which failed (Figures 21, 22, 25, and 27) does not show any variation in α. Alpha does not decrease but stays in the range of 0.60 to 0.68. No zero load loop width correction was required because Δ_{ps} was only measured at zero load. (The plastic strain computer only corrected for the total plastic strain and not the plastic strains for each row of joints separately). Several factors make it hard to determine the significance of the lack of variation in α for the single row displacement data. For one thing, there are only seven data points for the 25% and 50% load drop curves and only six points for the 90% and 100% load drop curves, versus about twice the number of points for the two row curves (as has been mentioned, the two row curves include data taken with only one extensometer spanning both rows). Furthermore, the shapes of the single row curves are largely controlled by a single displacement point at 6×10^{-4} in. This and the relatively few points limits any conclusions which can be drawn from this data. Furthermore, there is the added complication of the concentration in displacement which occurs as the test progresses.

It is clear that the definition of failure and the definition of the applied displacement both influence the data correlations. Multiple choices for these definitions have been made to reflect different possible uses for the data. The sum of the displacements of the two rows of joints is what is determined when the thermal mismatch between a chip carrier and circuit board is calculated. The data for the individual row of joints tells how the displacements are partitioned. The 25% drop in load criteria defines failure in terms of the initial stages of cracking. The 50% drop in load defines a somewhat later stage. The 90% drop in load defines a still later stage where the joint is severely damaged. Extrapolation to complete failure (100% load drop) is the least conservative definition of fatigue (i.e., gives the largest value for N_f) which represents an outer limit for design.

3.4 Coffin-Manson Low Cycle Fatigue Behavior: Resistance Increase Data

Figure 7 shows that the drop in load is accompanied by an increase in resistance. Fatigue can therefore be characterized by this joint resistance increase in the same way as it was characterized by the drop in load. There is, however, an important

difference. The resistance measurements describe the behavior of individual joints whereas the drop in load describes fatigue in terms of the average behavior of all the joints. It is clear from Section 3.1 that the distribution of cracking among the joints and shorting across the crack further complicates any exact correlation of the drop in load with the resistance increase of individual joints. Nonetheless, the study of the resistance increase of individual joints is an important measure of the fatigue process. This resistance increase is illustrated in Figures 31-38.

Figure 31 shows failure N_f defined by a joint resistance increase of only 0.02% for the *first* joint to increase this much. Resistance changes as small as 0.01% can be resolved, but such changes can be random. By the time the resistance increases to 0.02%, it denotes a situation where the joint resistance will continue to increase with subsequent fatigue cycling (as opposed to more random fluctuations below this level). Figure 31 shows, however, that there is a considerable amount of scatter when this small a resistance increase is used to define N_f. This is reflected in the wide 70% confidence band. The load drop was determined for each specimen at the point where the first joint reached a 0.02% increase in resistance. The average load drop where this occurred was 0.27 with a standard deviation of 0.25. This large variability reflects the variability in the initial cracking from one joint to another. Such a small resistance increase or a load drop of approximately 25% represents an early stage of joint failure – a stage which would not represent a truly compromised joint since there should be little electrical degradation for such a small resistance increase, and the decrease in the load bearing capability of the joints would not be very detrimental. The correlation of Figure 31 is with the load drop and the *first* joint to show a resistance increase of 0.02%. In this early stage in life, the behavior of the median joint is similar to that exhibited by the joint showing the maximum change in resistance (see Figures 14-16), but on average it correlates with a somewhat greater drop in load. The median joint reached a resistance increase of 0.02% when the load dropped by 0.43 ± .31. As with the maximum resistance increase data, there is a large amount of scatter associated with this small increase in resistance.

Figures 32 and 33 show the N_f values defined by the first joint to reach a 0.05% and 0.1% increase in resistance, respectively. The mean load drop values correlating with these resistance increases were 0.48 ± 0.21 and 0.63 ± 0.15, with Δ_p defined by the average of $\Delta_{p\,(max)}$ and Δ_p at half load. There was less scatter with these definitions of failure, as illustrated by the narrower 70% confidence limits and smaller standard deviation for the mean load drop. At a 0.05% increase in resistance, no crack was observed in the fillet. When the first joint reaches a resistance increase of 0.1%, a crack may be visible in the fillet. A median resistance increase of 0.05% correlates with an average load drop of 0.57 ± 0.24 and a median resistance increase of 0.1% correlates with an average load drop of 0.74 ± .14. Thus, while a crack may be visible in the most severely cracked joint when the load drops by 63%, it requires a

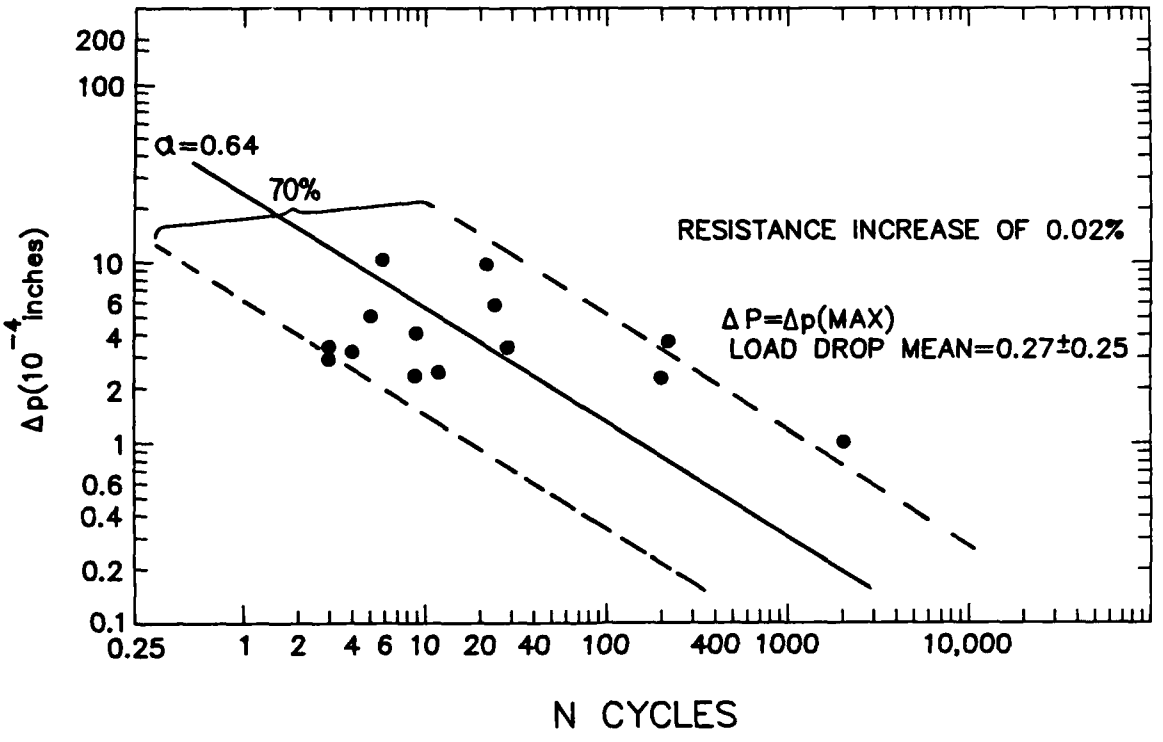

Figure 31. Displacement vs. fatigue life for the first joint showing a 0.02% resistance increase.

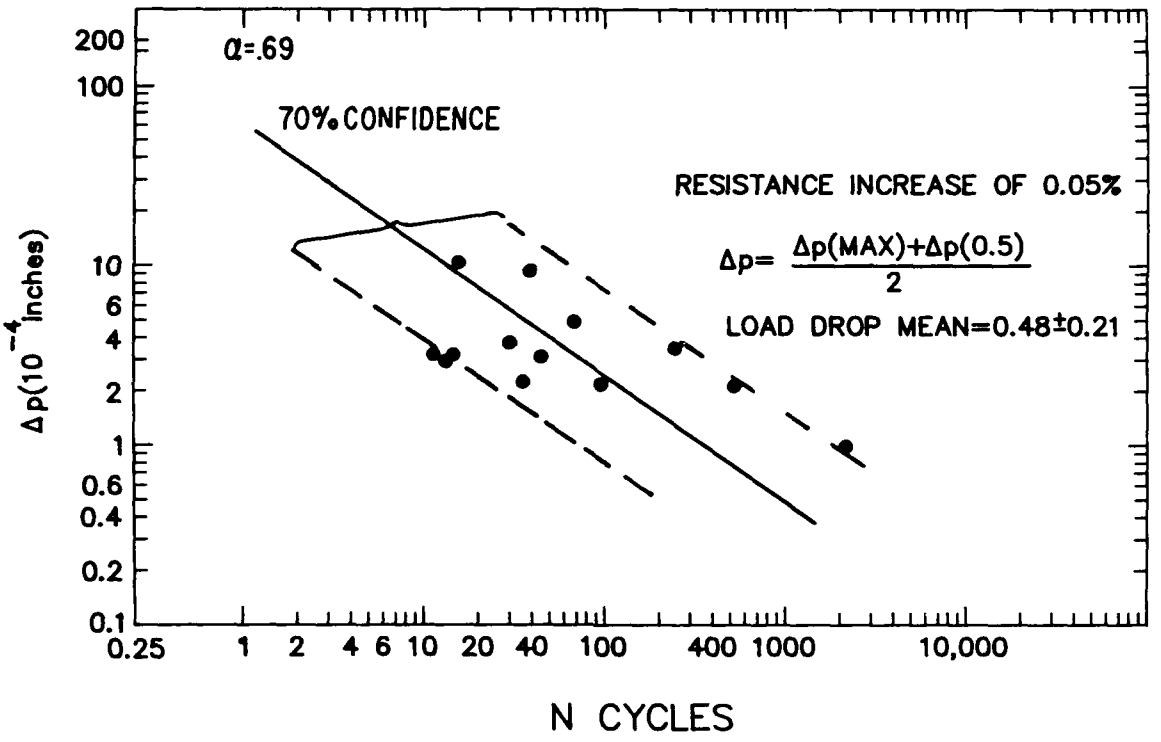

Figure 32. Displacement vs. fatigue life for the first joint showing a 0.05% resistance increase.

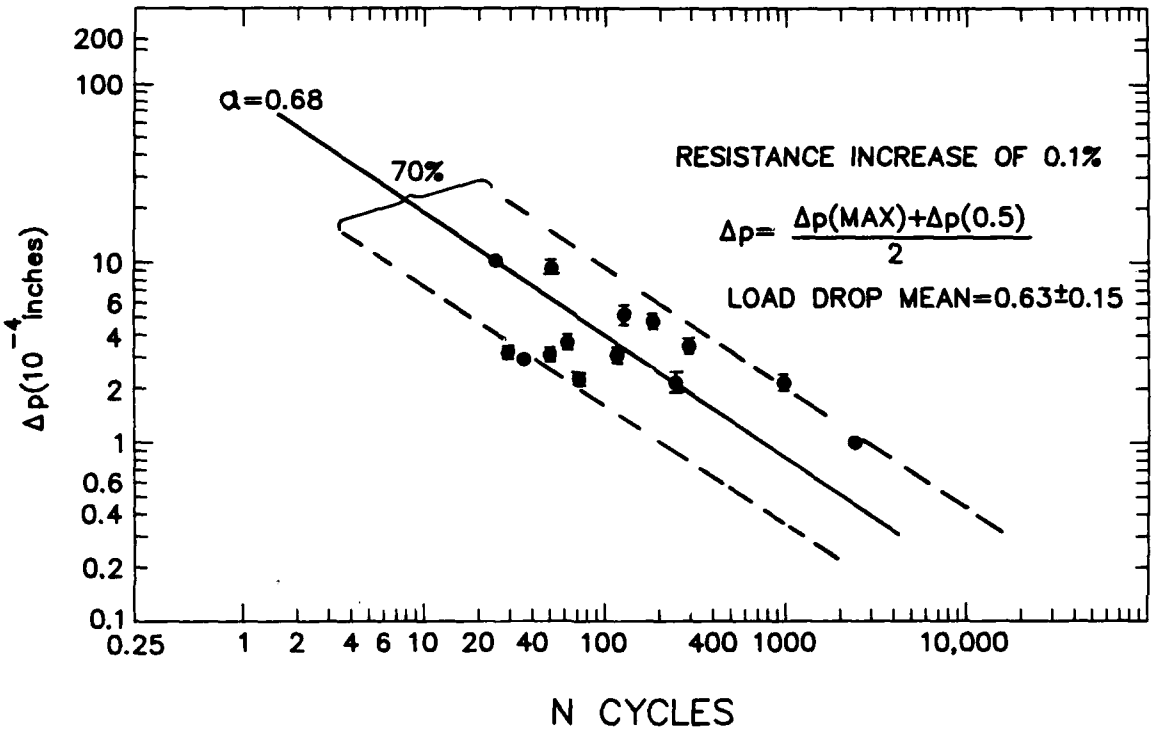

Figure 33. Displacement vs. fatigue life for the first joint showing a 0.1% resistance increase.

load drop of about 75% before the median joint should exhibit cracking.

Figures 34-37 show N_f as defined by the first joint to reach a resistance increase of 1%, 10%, 100%, and 10 times (1000%), respectively. The mean load drop values corresponding to these resistance increases were 0.82 to .88. The correlations with the 10%, 100%, and 10× resistance increase data were somewhat biased because many tests were stopped when the load drop reached about 90%, but before the resistance increase reached 10% in any joints. In these cases, the largest load drop reached was used in making the correlation between the resistance increase and load drop. This represents a lower bound for the load drop required to increase the resistance by 10%, 100%, or 10×, with the error introduced by this approximation increasing with the resistance increase correlation being made. As a general rule, however, when tests were run to a load drop of 95-98%, numerous joints showed open circuits (i.e., resistance increases of 10× or greater). At the worst, then, a resistance increase of 10× would therefore correlate with a load drop of 88 to 98%.

The resistance increase of the median joint of 1% or greater could not be determined because most tests were stopped before this occurred. At a 90% drop in load, the median joint reached a resistance increase of only 0.27% ± 0.16. While this was smaller than the resistance increase observed in the most damaged joint (which was about 10× on the average), it is large enough to be correlated with the presence of a visible crack in the fillet. While the resistance increase of the worst joint does not describe the average behavior (as does the median joint), its behavior is nonetheless very critical. It is the first joint failure which generally defines the device failure; hence a design life analysis must be based on this occurrence and hence its use in Figures 31-38.

Figure 38 correlates all the resistance increase curves. It could be used to estimate the fatigue life, based upon a number of resistance increase criteria, and by interpolation any resistance increase criteria between 0.02% to 1000% would be used to define failure. The slopes of the displacement vs. fatigue life curves are in the range of α = 0.69 to α = 0.52, and with the exception of the data for the 0.02% resistance increase (which exhibits the most scatter), α decreases with the larger the resistance increase used to define failure. This is similar to the behavior observed for the load drop curves, but with less of a decrease in α.

4. CONCLUSIONS

1. The fatigue cracking, resulting from the isothermal mechanical cycling of CC/PWB joints, starts below the chip carrier. With further fatigue cycling, the cracking extends into the fillet of the joint.

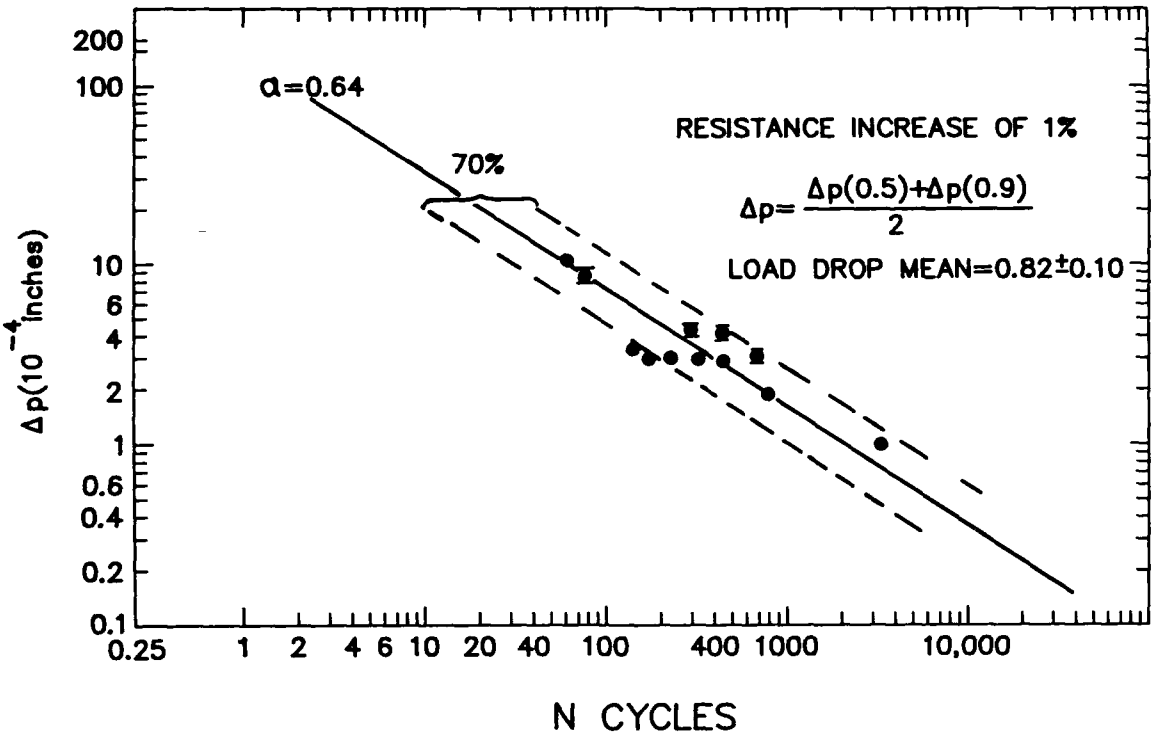

Figure 34. Displacement vs. fatigue life for the first joint showing a 1% resistance increase.

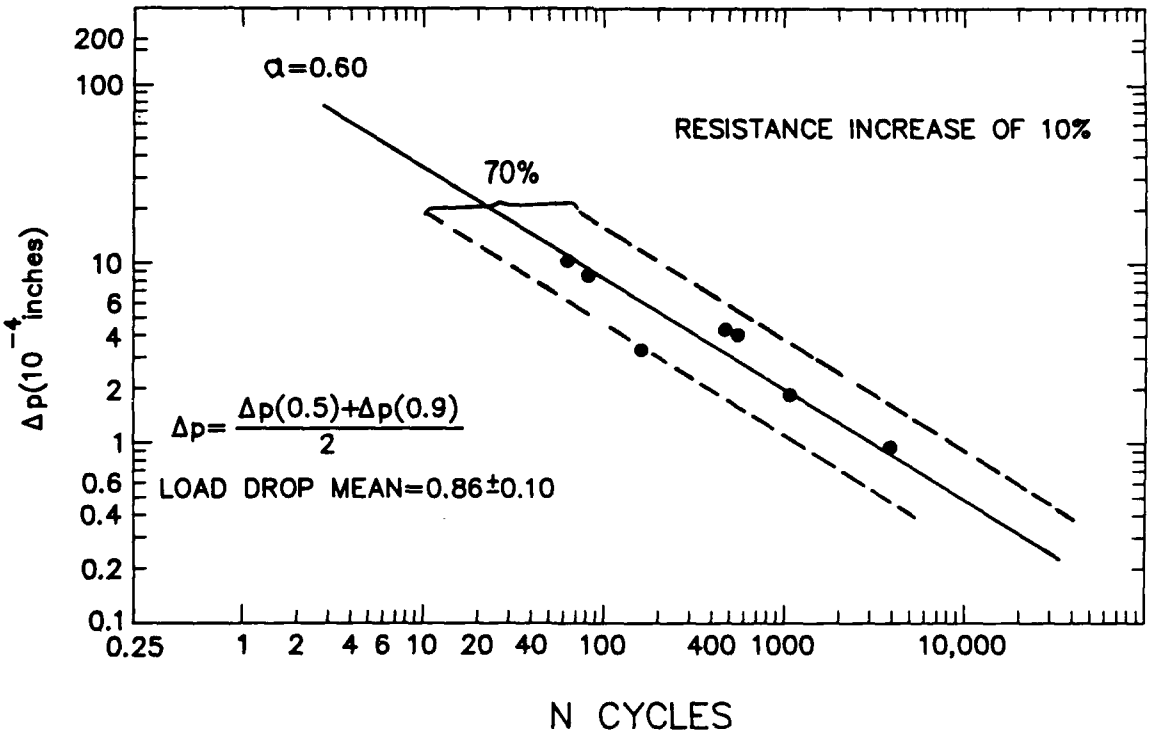

Figure 35. Displacement vs. fatigue life for the first joint showing a 10% resistance increase.

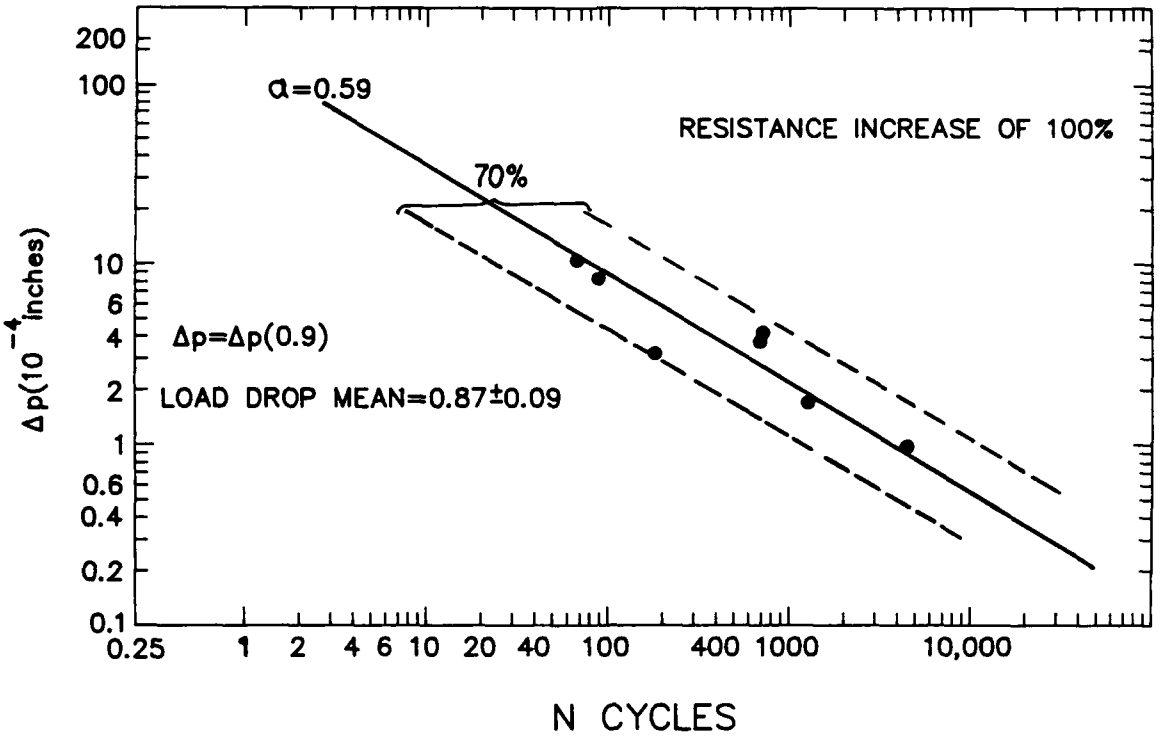

Figure 36. Displacement vs. fatigue life for the first joint showing a 100% resistance increase.

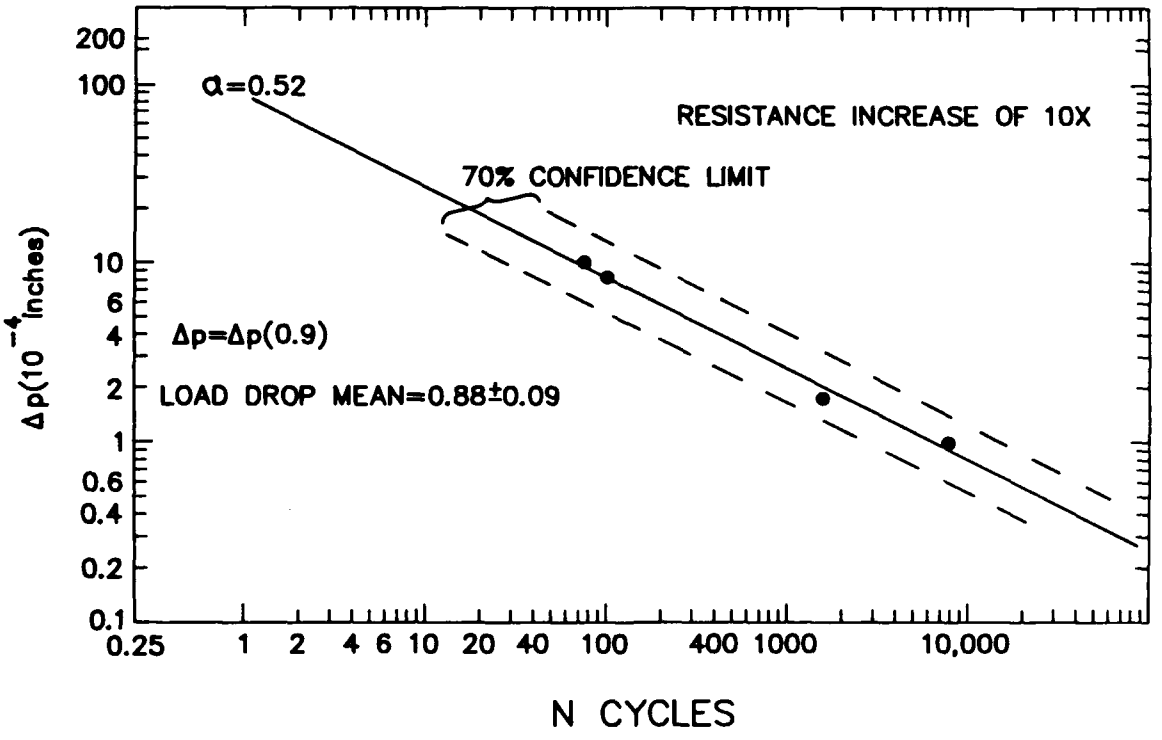

Figure 37. Displacement vs. fatigue life for the first joint showing a 10× resistance increase.

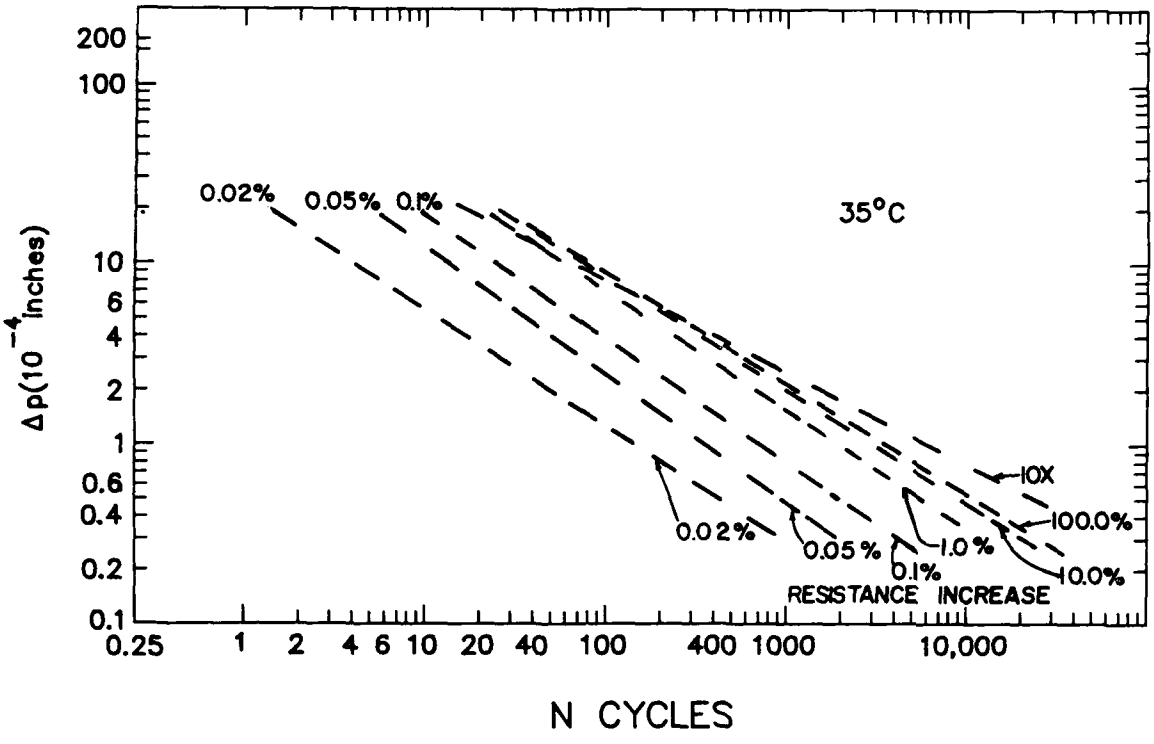

Figure 38. Summary of the displacement vs. fatigue life curves for different levels of resistance increase.

2. As the fatigue cycling progresses, the load required to produce a given displacement decreases and the resistance of the joints increases.

3. The rate of the load drop decreases with increasing cycling, whereas the rate of resistance increase increases with cycling. This behavior is explained in terms of the joint geometry.

4. A resistance increase of the first joint to increase by 0.02% corresponds to a load drop of about 25%.

5. A resistance increase of the first joint to increase by 0.05% corresponds to a load drop of about 50%.

6. It generally requires a 60-80% drop in load to produce a resistance increase of 0.1% or greater and for a crack to be optically visible on the surface of the fillet which shows the greatest resistance increase.

7. A resistance increase of 0.27% in the median joint correlates with a 90% drop in load. At this level, a crack should be visible in the fillet of this median joint.

8. When the drop in load exceeds 60-80%, one joint will exhibit a much larger resistance than the others and the spread in behavior will increase as the cycling continues. Thus, when the median joint only displays a 0.27% resistance increase (at a 90% drop in load) the resistance in the worst joint has, on the average, increased by 10×.

9. Bending of as much as 10^{-3} deg/lb did not influence the fatigue life.

10. The fatigue life N_f was described in terms of a pseudo Coffin-Manson Law with N_f being related to the plastic displacement instead of the plastic strain. The plastic strain developed in the joint is a function of the imposed displacement, but it is very non-uniform.

11. The slope of the pseudo Coffin-Manson curve is similar to that observed when the plastic strain is used instead of the plastic displacement. The slope is, however, to some degree dependent upon how the displacement is measured and the degree to which fatigue cracking has progressed through the joints.

12. Numerous pseudo Coffin-Manson curves are provided so that the fatigue life can be determined for a wide variety of failure criteria and definitions of the applied plastic displacement.

ACKNOWLEDGMENTS

The author would like to thank John DeVore (GE E-Lab, Syracuse, NY) for the metallography performed with respect to Figures 8 and 12, and Bill McFarland (GE-CRD) for his statistical determination of the trend lines and confidence limits. The

author gratefully acknowledges fruitful discussions with John DeVore, Bill McFarland, Walt Pillar (GE - AESO, Utica), and Bill Fahy (GE-AESD, Utica)

This work was performed under AF Contract #F33615-85-C-5065. The author is grateful for this support and for the support given by Don Knapke, Preston Opt, and Ed Morrisey, all of the AF Materials Lab (WPAFB, Ohio).

REFERENCES

[1] T.H. Lau and D.W. Rice, Solid State Technology, V. 28, pp. 91-104 (1985).

[2] H.D. Solomon "Low Cycle Fatigue of 60/40 Solder-Plastic Strain Limited vs. Displacement Limited Testing" in Electronic Packaging: Materials and Processes, Ed. J. A. Sortell, ASM, 1986, pp. 29-49.

[3] H.D. Solomon, "Low-Frequency, High-Temperature Low-Cycle Fatigue of 60Sn/40Pb Solder" in ASTM – STP 942, Ed. H. D. Solomon, et al., 1987, pp. 342-369.

[4] H.D. Solomon, Brazing and Soldering, No. 11, pp. 68-75 (1986).

[5] H.D. Solomon, IEEE-CHMT-9, pp. 423-433 (1986).

[6] R.N. Wild, Welding J., V. 51, 5215-5265 (1972).

[7] W. Engelmaier, IEEE-CHMT-6, pp. 232-237 (1983).

[8] J.K. Lake nd R.N. Wild, 28th National SAMPE Symposium, pp. 1406-1414 (1983).

[9] P.M. Hall, IEEE-CHMT-7, pp. 314-327 (1984).

[10] D. Stone, S.P. Hanula and C.Y. Li, IEEE – 35th ECC, May 1985.

[11] G.V. Clatterbaugh and H.K. Charles, Jr., ISHM 85, pp. 31-42 (1985).

[12] K.E. Felske and T. Moss, IEEE - 36th ECC, pp. 641-648, (1986).

[13] L.F. Coffin, Jr., Trans. ASME, V.76, pp. 931-950 (1954).

[14] S.S. Manson, "Behavior of Materials Hinder Conditions of Thermal Stress" in Heat Transfer Symposium, University of Michigan Press (July 1953).

[15] S.S. Manson, Experimental Mechanics, V.5, pp. 193-226 (1965).

[16] L.F. Coffin, Jr., Proc. Inst. Mech. Eng., V.188, pp. 109 (1974).

[17] L.F. Coffin, Jr., Proc. ASTM-STP520, pp. 5-34 (1973).

[18] H.D. Solomon, to be published.